Structure, origin, and deformation of the lithosphere in the northern Canadian Cordillera from high-resolution, passive-source seismic velocity models

C. Estève[1], P. Audet[2], D. L. Schutt[3], R. C. Aster[3], A. J. Schaeffer[4], and Joel F. Cubley[5]

[1]Department of Meteorology and Geophysics, University of Vienna, Vienna, Austria
[2]Department of Earth and Environmental Sciences, University of Ottawa, Ottawa, Ontario, Canada
[3]Department of Geosciences and Warner College of Natural Resources, Colorado State University, Fort Collins, Colorado, USA
[4]Geological Survey of Canada, Pacific Division, Natural Resources Canada, Sidney, British Columbia, Canada
[5]Centre for Northern Innovation in Mining, Yukon University, Whitehorse, Yukon, Canada

Corresponding author: Clément Estève, `clement.esteve@univie.ac.at`

Abstract

The recent deployment of temporary broadband seismic networks, notably the EarthScope USArray-Transportable Array (TA), has drastically improved the station coverage across northwestern Canada over the last ten years, enabling application of high-resolution passive-source seismic methods (*i.e.,* seismic tomography, receiver functions and core phase shear wave splitting). This review highlights the main discoveries pertaining to the seismic velocity structure, origin and deformation of the lithosphere in the northern Canadian Cordillera (NCC). High-resolution seismic tomography models reveal that the lower crust in the NCC is marked by low velocity anomalies extending from the Gulf of Alaska to the Cordilleran deformation front, which is interpreted to reflect elevated temperatures that buoyantly support regional high elevations and potentially represent the seismic signature of strain transfer from the Yakutat collision zone to the Mackenzie Mountains. The Moho is relatively flat and shallow across the NCC, and is underlain by a thin layer of mantle lithosphere. Seismic velocity models further unveiled large-scale mantle structures associated with the unexposed Mackenzie craton in the north, and the Liard Transfer Zone in the south, which appear to buttress the NCC and further focus deformation in the eastern NCC. Seismic anisotropy and tomography provide evidence that the Tintina and Denali faults penetrate into the lithospheric mantle and played a first order role in shaping the present-day NCC. We propose that future studies should aim to: 1) resolve the shape of the Cordillera-craton boundary at upper mantle depths; 2) accurately estimate the lithosphere thickness in the NCC; and 3) improve coverage in the Beaufort Sea to understand the controls on convergent tectonics in the northern NCC.

1 Introduction

The geological history of western Canada spans 4 billion years, from juvenile terranes accreted along the Pacific Ocean margin to Archean rocks of the Canadian Shield (Gabrielse & Yorath, 1991). Recent reviews of the geology, structure and metallogeny of the Cordillera can be found in Colpron et al. (2007) and Nelson et al. (2013). Here we provide a brief review of the macro-scale features that can be targeted by passive-source broadband seismic networks. The Canadian Cordillera is a ∼500-800 km-wide Phanerozoic mountain belt that extends from the US border in the south to Alaska and the Beaufort Sea in the north. To the east, the Canadian

Cordillera is flanked by Proterozoic magmatic arcs and the Archean Canadian Shield. To the west, plate boundary interactions vary from south to north. In southwestern Canada, the oceanic Juan de Fuca plate subducts beneath the North American plate at the Cascadia Subduction Zone. Northward, the margin is characterized by transpressive to strike-slip motion between the Pacific and North American plates along the Queen Charlotte-Fairweather fault system. Further north, the Yakutat block is colliding obliquely with the North American margin in the Gulf of Alaska, producing the fastest rising and highest elevations in Canada within the St. Elias-Chugach mountain ranges.

The Canadian Cordillera can be broadly separated into northern (NCC) and southern (SCC) zones based on differences in surface geology, tectonics, and contemporary geodynamics. This separation approximately aligns with the Yukon-British Columbia border (latitude 60°N), and is demarcated by a clear change in seismicity (Fig. 1). Seismic activity is well observed to the north within the NCC, and is mainly focused at the plate boundary margin and at the Yakutat collision zone (Cassidy et al., 2005; Ristau et al., 2007). However, seismicity is also abundant within the Mackenzie Mountains and in the Richardson Mountains, ∼800 km away from the nearest plate boundary. In contrast, seismicity is almost absent in the SCC, with modest clusters of seismic activity located to the east within the foreland basin. This north-south transition roughly occurs at the Liard transfer zone (LTZ; Fig. 1), a tectonic structure inherited from the asymmetric Neoproterozoic rifted margins of Laurentia that separates a southern upper-plate margin from a northern lower-plate margin (Lund, 2008). The extension of the LTZ into the NCC coincides with the Liard Basin, located at the nexus of the NCC Tintina Fault and the SCC Rocky Mountain Trench. The Tintina fault is a margin-parallel right-lateral strike slip fault that accommodated ∼430 km of horizontal displacement between late Eocene and Early Cretaceous (Gabrielse et al., 2006) but displays low seismic activity. North of the NCC, earthquake focal mechanisms and sparse geodetic data (Leonard et al., 2007; Mazzotti et al., 2008) suggest that the Yukon crust is slowly converging (∼2 mm yr^{-1}) with the Beaufort sea margin, which may lead to, or reflect, subduction initiation (Hyndman, et al., 2005).

Much of our knowledge of deep Cordilleran crust and mantle structure was gained from three deep magnetotelluric and controlled-source seismic profiles that were acquired as part of the Slave-Northern Cordillera Lithospheric Evolution transect (SNORCLE; Figure 1) from the

Lithoprobe project (Cook & Erdmer, 2005). Data collected by SNORCLE led to the discovery of several crustal-scale features in the NCC. First, the identification of a reflective westward tapering wedge within the Cordilleran crust west of the Tintina Fault was interpreted as the seismic signature of Proterozoic meta-sedimentary strata in the middle and lower crust beneath the Cordillera. This led to the hypothesis that the deep tapered wedge originated as sediments deposited in a passive margin setting. Under this scenario, most of the Cordilleran terranes are thin sheets thrust over older ancient North American basement. Second, seismic profiles showed a nearly flat and shallow Moho, indicating that crustal thickness does not vary much along the profiles despite topographic variations. This was a surprising result since the age of surface rocks and topographic elevations vary widely from Archean to Cenozoic and from near sea level to more than 2,500 m along east-to-west profiles, respectively (Cook & Erdmer, 2005). This finding led to the suggestion that thermal processes have largely erased crustal thickness variations through lower crustal ductile flow or partial melting (Cook, 2002). Seismic velocity models derived from SNORCLE seismic refraction data also revealed a westward Proterozoic meta-sedimentary wedge directly to the west of the Tintina Fault and a flat Moho at ∼33–36 km depth (Clowes et al., 2005). Magnetotelluric data from SNORCLE revealed complex electrical resistivity structure throughout the NCC (*e.g.,* Ledo et al., 2002; Jones et al., 2005). Recently, Dehkordi et al. (2019) reprocessed the available Lithoprobe SNORCLE magnetotelluric data from 69 instruments along Line 2 and the resulting 2-D resistivity model showed significant variations within the crust on both sides of the Tintina Fault and beneath the LTZ. The authors suggest that the Tintina Fault may have juxtaposed two crustal blocks from the lower- and upper plate margins.

Following SNORCLE, there was a long hiatus in geophysical infrastructure development. Geophysical advances following SNORCLE were made using potential field data, heat flow measurements, seismicity data as well as campaign and continuous Global Navigation Satellite System (GNSS) data from surveys led by the Geological Survey of Canada. Most notably, those studies revealed that: 1) the entire NCC is characterized by low effective elastic thickness (T_e) and low Curie depth, implying a hot and weak crust (Flück et al., 2003; Audet et al., 2007; Gaudreau et al., 2019); 2) the Mackenzie Mountains are buttressed by rigid crustal blocks inferred from magnetic anomaly data (Saltus & Hudson, 2007); 3) heat flow is high throughout the NCC (Lewis et al., 2003); and 4) strain transfer from the Yakutat collision zone may drive deforma-

tion across the NCC all the way to the Cordilleran Deformation Front (CDF) (Mazzotti & Hyndman, 2002).

Two distinct tectonic models were developed to explain these observations, with the aim to describe contemporary deformation of the Cordillera and predict the role of the upper mantle. First, based on the orogenic float model of Oldow et al. (1990), Hyndman, et al. (2005) proposed that thermal expansion in the upper mantle buoyantly supports the high elevation (mean value of ∼1000 m above sea level) across the entire Canadian Cordillera. High Moho temperatures (∼ 900°C) give rise to zones of weakness in the lower crust and this helps to propagate stresses from the Yakutat collision zone that drive seismic activity in the Mackenzie Mountains (Mazzotti & Hyndman, 2002). This model inherently requires crust-mantle mechanical decoupling along a lower crustal detachment zone at the base of a thin crust (Hyndman, 2017), and therefore a minimal role of the upper mantle in controlling deformation. Alternatively, Finzel et al. (2015) modeled mantle convection across Alaska and the northern Canadian Cordillera and proposed that the current stress pattern can be explained by traction at the base of the lithosphere; this implies crust-mantle mechanical coupling, and therefore an important role for the upper mantle. Additional tectonic models were proposed to explain magmatism in the Northern Cordilleran slab window (Thorkelson et al., 2011), which implies retreating lithospheric support beneath the margin and potential destabilization of the Cordilleran lithosphere (*e.g.,* Currie et al., 2008).

Further evaluation of these models requires accurate representations of the structural makeup and architecture of the lithosphere and upper mantle beneath the NCC and surrounding regions. This information is most readily extracted from high-resolution seismic velocity models determined using broadband seismic data; unfortunately, the historical lack of a dense, passive, broadband seismograph network in northwestern Canada has hampered the development of such models until very recently. The first few seismograph stations in northwestern Canada were installed in the 1990s by the Canadian federal government to monitor earthquake activity across the country. Until the early 2000s, station coverage remained sparse with only a handful of seismic stations deployed in the NCC (Fig. 2). In 2003, the temporary CAnadian NOrthwest Experiment (CANOE, https://doi.org/10.7914/SN/XN_2003) seismograph network was deployed for two years. Over time, seismic station coverage continued to improve across the region, with a sig-

nificant expansion starting in the 2010s. The Yukon-Northwest Territories Seismograph Network (https://doi.org/10.7914/SN/NY) as well as the Yukon Observatory network were installed in 2013 and 2016, respectively. 2017 marks the year of completion of the deployment of the EarthScope USArray TA (hereinafter referred to as TA) geophysical observatories across Alaska, USA and Yukon, Canada (Busby & Aderhold, 2020). Between 2016 and 2018, the Mackenzie Mountains EarthScope Project was deployed for two years along a SW-NE NCC-crossing profile (Baker et al., 2019).

Recent improvement in seismograph station coverage across northwestern Canada has enabled the use of a wide variety of seismic imaging techniques (i.e., ambient noise and earthquake-based surface-wave tomography, as well as regional and teleseismic body-wave tomography) to investigate the three-dimensional crustal and upper mantle seismic velocity structure at higher resolution. Body-wave travel-time models generally have better lateral resolution compared to surface wave methods due to crossing near-vertical and bending rays, but suffer from reduced vertical resolution due to limited ray path coverage and direction. Conversely, surface-wave models provide coverage along horizontal paths with generally lesser horizontal resolution. Other complementary models providing more localized estimates of crust and upper mantle structure were also utilized from these new data sets (e.g., receiver functions, teleseismic shear-wave splitting). Taken together, these recent studies have led to new discoveries and geodynamic model testing while simultaneously raising further questions about the past and present tectonics of this region. In this review, we provide a summary of passive-source seismological studies across the NCC, Alaska, and northwestern Canada, and propose ongoing research questions for the region.

2 Seismic velocity structure of the crust

2.1 3-D seismic velocity models

The first 3-D shear-wave velocity model of the crust in northwestern Canada was calculated by Dalton et al. (2011) using fundamental mode, group velocity Rayleigh and Love wave dispersion measurements at periods of 7–20 s from ambient noise data mainly recorded by the CANOE network. They found that: 1) low-velocity regions spatially correlate with known sed-

158 imentary basins at shallow crustal depths (< 5 km); and 2) at mid-crustal depths, there are sev-
159 eral low-velocity zones within the western part of the Canadian Shield that extend beneath the
160 NCC, which may reflect the westward tapering Proterozoic meta-sedimentary layers inferred from
161 SNORCLE (Snyder et al., 2002). Unfortunately, this data set did not allow for high-resolution
162 imaging of the lower crust and lithospheric mantle. In 2013, Kao et al. (2013) developed the first
163 pan-Canadian S-wave velocity model of the crust and uppermost mantle obtained from ambi-
164 ent noise data (Figs. 3a-b and 4a-b). They found that the Cordilleran crust is characterized by
165 low seismic velocities with large vertical S-wave velocity gradients at upper- to mid-crustal depths,
166 speculated to represent the seismic signature of ductile detachments within the middle crust,
167 e.g., consistent with the geodynamic hypothesis of Mazzotti and Hyndman (2002). However, only
168 a handful of stations were used in the NCC and these large vertical S-wave velocity gradients
169 are not present everywhere in the Cordillera, which made this interpretation tentative.

170 Prior to the roll-out of the TA into parts of the Yukon, McLellan et al. (2018) incorporated
171 the then recently-available YNSN data and developed fundamental mode Rayleigh-wave phase-
172 velocity maps of northwestern Canada using ambient noise and teleseismic data at periods be-
173 tween 8 and 80 s. They found that low phase velocities at periods < 25 s are confined to the
174 NCC between the Tintina Fault and the CDF. Known sedimentary basins (e.g., the Selwyin Basin
175 that encompass most of eastern Yukon, and the Liard Basin in southeastern NCC) are charac-
176 terized by low-velocity anomalies at periods $\leq$ 15 s (Fig. 3g). Southwest of the Denali fault,
177 another low-velocity anomaly was interpreted as the signature of underplated sediments at the
178 base of the Chugach terrane (Ward, 2015; McLellan et al., 2018) due to the Yakutat flat-slab
179 subduction. At mid- to lower-crustal depths, the Mackenzie Mountains were found to be under-
180 lain by a broad low-velocity feature (Fig. 3g-h). Higher resolution surface-wave tomography mod-
181 els refined these features by including data from the TA and Mackenzie Mountains EarthScope
182 Project (Baker et al., 2019). Estève et al. (2021) showed that an anomalous low S-wave veloc-
183 ity structure ($\delta V_S < -3\%$) extends from the Pacific Ocean to the CDF, with the Mackenzie
184 Mountains being underlain by a large low-velocity anomaly (Figs. 3c-d, 4c-d). Schutt et al. (2023)
185 inverted ambient seismic noise-derived surface wave data between 6–40 s period to further re-
186 solve the lithospheric S-wave velocity beneath the Mackenzie Mountains and confirmed the pres-
187 ence of a large low-velocity anomaly beneath this area with a westward dip. This S-wave ve-

188 locity model highlights the transcrustal continuity of this seismically slow region into the up-
189 permost mantle (see section 4.5). Lastly, a 10–15 km-thick, low-velocity layer with variable am-
190 plitude can be traced at lower crustal depths everywhere across the NCC (Figs. 3e-f, 4e-f).

191 Those aforementioned seismic tomography models have different levels of resolution. For
192 instance, Kao et al. (2013) show that their model resolves features of $\sim$ 100–200 km in dimen-
193 sion at short periods in western Canada. However, the resolution falls off for longer periods (*i.e.,*
194 35s, 200-300 km; 50s, 250-500km). Structures revealed by the tomography models of McLellan
195 et al. (2018) with minimum dimensions of 200x200 km can be confidently interpreted within the
196 NCC. However, their model is biased by dominant east-west path coverage due to the geome-
197 try of the seismic network, noise source locations and earthquake locations. The recent tomog-
198 raphy models of Estève et al. (2021); Schutt et al. (2023) accurately recover features with a 300
199 km lateral extent.

200 ### 2.2 Moho depth model

201 Prior to the SNORCLE experiment, only sparse Moho depth estimates were available for
202 the NCC. Lowe and Cassidy (1995) calculated P receiver functions and showed that the Moho
203 is shallower beneath Dawson City than beneath Whitehorse, Yukon. Results from the Litho-
204 probe SNORCLE experiment highlighted a relatively shallow ($\sim$33–35 km) and flat Moho along
205 the profiles (Clowes et al., 2005). These and other Lithoprobe results were interpolated to cre-
206 ate the first Moho map of Canada at 5$\times$5 degrees (Perry et al., 2002). A decade later, Rasendra
207 et al. (2014) calculated P receiver functions for 11 broadband seismic stations near the Denali
208 Fault in southwestern Yukon. Their results indicated a $\sim$4 km shallower Moho ($\sim$36 km) be-
209 neath stations located north and east of the Denali Fault compared to those located south and
210 west ($\sim$39–40 km), which correlates with topographic variations across the Denali fault. Prior
211 to the completion of the TA network, Tarayoun et al. (2017) calculated P receiver functions for
212 stations of the YNSN, CN, CANOE and the first nine stations of the USArray TA EarthScope
213 network in northwestern Canada and obtained Moho depth estimates using both the H-κ stack-
214 ing technique and the harmonic decomposition method. Their results confirmed a sharp and nearly
215 flat Moho across the NCC (mean of 32 $\pm$ 2 km), in good agreement with prior studies (*e.g.,* Clowes
216 et al., 2005; Rasendra et al., 2014). Subsequently, Audet et al. (2019) used receiver functions

to image the Moho along the western transect of the CANOE line from the CDF to Whitehorse, Yukon, and found similar results.

Audet et al. (2020) expanded on these results and investigated Moho depth variations across the entirety of the NCC with all available seismic stations (total of 173), including those belonging to the TA and the Mackenzie Mountains EarthScope Flexible Array seismic networks (Fig. 5). They obtained Moho depth estimates ranging from 27 to 43 km with a mean value of 33 km, again consistent with previous studies (Clowes et al., 2005; Rasendra et al., 2014; Tarayoun et al., 2017; Audet et al., 2019). The authors observed that seismic activity is partially correlated with areas exhibiting a Moho deeper than 36 km. These areas are southwest of the Denali Fault beneath the actively deforming St. Elias-Chugach Mountains, the northwestern part of the Mackenzie Mountains and the Richardson Mountains. It is intriguing to note that, north of the Tintina Fault, the Mackenzie Mountains EarthScope Project Flexible Array marks the limit between a shallower Moho (∼28–30 km) across the southern Mackenzie Mountains compared to their northern counterpart (∼40 km). If this observation were robust, it would imply a revision of the geological models of the deep Cordilleran crust and its evolution through time. However, this observation is inferred from interpolation of results with only a few stations, with large observational gaps on either side of the Mackenzie Mountains array. This highlights the need for additional instrumentation to fill the gaps in the current coverage.

2.3 Crustal seismic anisotropy

Estimates of seismic anisotropy within the crust inform the state of stress and/or large-scale tectonic fabrics. These estimates are typically obtained from either the inversion of surface-wave dispersion data, receiver functions or, for the shallowest crust, microseismicity shear-wave observations (*e.g.,* Aster & Shearer, 1992). Estimates of bulk crustal seismic anisotropy from receiver function data suggest the existence of a fabric with a fast-axis direction of propagation oriented to the NW-SE, consistent with the orientation of the Denali and Tintina faults (Rasendra et al., 2014; Tarayoun et al., 2017). Azimuthal anisotropy inferred from surface-wave tomography models (McLellan et al., 2018; Estève et al., 2021; Schutt et al., 2023) shows a similar NW-SE oriented large-scale pattern across the NCC at periods of 15 to 20 s, which are predominantly sensitive to crustal structure (Fig. 6). These results suggest a dominant tectonic fabric caused

by large-scale motion of the crust, possibly related to the Mesozoic accretion of terranes in the NCC (*e.g.,* Johnston, 2008) and/or the crustal shearing caused by the large right-lateral fault network (Denali, Teslin and Tintina faults) across the NCC. Improving crustal seismic anisotropy models remains a focus for future studies.

First-order patterns of azimuthal anisotropy derived from surface wave tomography models across the NCC are similar. However, one can note a clear difference in amplitude between the study of McLellan et al. (2018) and Estève et al. (2021); Schutt et al. (2023). This difference could arise from different choices of parameterizations. McLellan et al. (2018) utilize a linearized and regularized inversion, where the results depend strongly on the choice and level of regularization. Estève et al. (2021) and Schutt et al. (2023) use the same Bayesian trans-dimensional tomographic approach, which presents the advantage of avoiding model regularization. It has been shown that regularization of azimuthal anisotropy and quantifying uncertainties in surface wave tomographic inversions are challenging (Gosselin et al., 2021). Nonetheless, resolution of the anisotropic component is similar to that of the isotropic component of the tomographic inversion (McLellan et al., 2018). The uncertainty of anisotropy fast-axis directions (σ_θ) calculated by Estève et al. (2021) ranges between a few degrees and 30° within the NCC, except for the central part of the Mackenzie Mountains, where $\sigma_\theta > 30°$. σ_θ values across the NCC from Schutt et al. (2023) are smaller compared to Estève et al. (2021) ($0° \leq \sigma_\theta < 25°$). Differences may arise from a better path coverage using ambient noise data compared to regional earthquake data.

3 Seismic velocity structure of the upper mantle

3.1 3-D body-wave velocity models

Studies of the northern Canadian Cordillera upper mantle velocity structure started in the late 1970s using short-period P-waves, surface waves and long-period S-wave travel-time residuals (Buchbinder & Poupinet, 1977; Wickens, 1977; Wickens & Buchbinder, 1980). These studies suffered from sparse station coverage and thus low resolution, but revealed low velocities and delayed residuals to the west of the CDF. The continental-scale S-wave velocity model of Grand (1994) was the first to image the Canadian mantle. This model showed that the entire North

American Cordillera is underlain by low S-wave velocities down to ∼100 km. Following the work of Grand (1994), various continental-scale body-wave velocity models were developed (*e.g.,* Schmandt & Lin, 2014), although most focused on the conterminous US and did not provide new insight on the Canadian Cordilleran mantle.

At the regional scale, Frederiksen et al. (1998) developed the first teleseismic P-wave tomography model of the NCC from relative arrival-time data using 17 seismic stations from the gulf of Alaska to Yellowknife, Northwest Territories. Their model revealed: 1) a low-velocity anomaly in southwestern Yukon, interpreted to reflect an upwelling of hot material caused by the opening of a slab window at 20-30 Ma (Thorkelson et al., 2011); and 2) the Cordillera-craton boundary may be located west of the Tintina Fault. Taking advantage of several temporary seismic network deployments, Mercier et al. (2009) developed teleseismic P- and S-wave tomography models across western Canada using a similar technique. Their models revealed a sharp transition between low- and high-velocity anomalies across the CDF in the NCC, interpreted to be the boundary between the Cordilleran and the cratonic mantle. Estève et al. (2019) later developed new P- and S-wave teleseismic body-wave models of northwestern Canada that encompassed the south-easternmost part of the NCC, and obtained results similar to Mercier et al. (2009).

Expansion of the seismic networks in the 2010s, most notably the EarthScope TA, facilitated the development of new high-resolution body-wave velocity models in the NCC. Estève et al. (2020b) used all available data from 320 broadband seismic stations located across northwestern Canada and eastern Alaska to produce new teleseismic P- and S-wave velocity models of the upper mantle, also based on relative arrival time data (Fig. 8). Most notably, these models revealed the juxtaposition of several high- and low-velocity anomalies at depths between 100 and 300 km beneath the NCC. The largest features include the high P-wave velocity anomalies buttressing the ends of the Mackenzie Mountains beneath the NCC, and the sharp changes from positive to negative P-wave velocity and S-wave velocity anomalies across the Tintina Fault. Several of these features are limited to depths ≤200 km, and unveil the fine-scale structure of the upper mantle beneath the NCC. Recently, Boyce et al. (2023) re-processed multiple teleseismic body-wave relative arrival-time data sets and developed an absolute teleseismic P-wave velocity model of North America, which confirmed the results of Estève et al. (2020b) in the NCC.

3.2 3-D surface-wave velocity models

The first continental-scale surface-wave seismic velocity models of North America by Frederiksen et al. (2001) provided the most detailed regional constraints on upper mantle structure beneath the NCC at that time. This model displayed consistent low S-wave velocities at upper mantle depths beneath the entire Canadian Cordillera. The slow expansion of the seismic network in northwestern Canada allowed refinements of these continental-scale models over time (*e.g.,* van der Lee & Frederiksen, 2005; Bedle & van der Lee, 2009); however, new insights on upper mantle structure beneath the NCC were limited. Following the completion of the TA network over the conterminous US, Schaeffer and Lebedev (2014) developed a continental-scale S-wave velocity model of the North American upper mantle using multi-mode surface-wave data from the US-Array and other global seismic networks. Their velocity model highlighted several features. In particular, the transition between low- and high-velocity anomalies in western Canada is characterized by a sharp velocity gradient beneath the surface expression of the Rocky Mountain Trench, in good agreement with Mercier et al. (2009). Further north, within the NCC, the eastern region of the Mackenzie Mountains and the Richardson Mountains are characterized by a high-velocity anomaly and the transition to the low-velocity anomaly lies further west, between the Tintina Fault and those mountain ranges.

The development of regional-scale surface-wave velocity models of northwestern Canada took advantage of the sudden increase in network coverage in the mid 2010s. For instance, Zaporozan et al. (2018) applied the two-station surface-wave interferometry technique of Meier et al. (2004) using the permanent stations of the CN network as well as temporary stations from the POLARIS network to map Rayleigh wave phase velocities across western Canada. Once again, their velocity model highlighted the sharp seismic velocity contrast between low-velocity Cordilleran mantle and high-velocity cratonic lithosphere. Interestingly, their transects through their S-wave velocity model showed dip variations of the sharp velocity contrast from north to south. McLellan et al. (2018) used the same technique but focused on the NCC only and incorporated legacy data from the CANOE and POLARIS network as well as new data from the YNSN and a handful of TA stations in northwestern Canada. Their long-period (40–80 s) surface-wave model indicates extension of high phase velocity anomalies beneath the NCC, east of the Tintina Fault. More recently, the surface-wave models of Estève et al. (2021) and Schutt et al. (2023) have pro-

vided further constraints on shallow upper-mantle structure, as mentioned previously. Notably, they find significant velocity variations to the west of the CDF (Figs. 7b-c).

3.3 Layered structure

Although the new seismic body-wave and surface-wave models afford an unprecedented view of the upper mantle beneath the NCC, they are generally insensitive to discontinuities in seismic velocity related to fine-scale structural layering of the lithosphere. Tarayoun et al. (2017) used receiver functions, which are sensitive to discontinuities, and identified a 10 km-thick, high-velocity, anisotropic sub-Moho NCC layer at 40–45 km depth, which was tentatively interpreted as the signature of a thin lithospheric mantle. Audet et al. (2019) reprocessed receiver functions along the western transect of the CANOE line using common conversion point stacking to image the layered structure beneath the NCC. This study confirmed the existence of a high-velocity layer directly beneath the Moho discontinuity, interpreted to represent thin lithospheric mantle, estimating the thickness of the mantle lithosphere to be 15±3 km and the total lithosphere thickness as 50±5 km. This imaging also unveiled a west-dipping feature in the uppermost mantle, compatible to that observed in the surface wave model of Schaeffer and Lebedev (2014) and analogous to observations from the southern Canadian Cordillera by Chen et al. (2019). However, the origin and longevity of this feature remains enigmatic.

3.4 Upper-mantle seismic anisotropy

Seismic anisotropy in the upper mantle is principally attributed to stress- or strain-induced alignment of olivine which may reflect present-day mantle convection and/or "fossil" deformation in the upper mantle (Savage, 1999; Park & Levin, 2002; Becker & Lebedev, 2021; Hansen et al., 2021). Teleseismic shear-wave splitting estimates (mainly from SKS and $SKKS$ core phases) in the NCC resolve an alignment between the fast axis of azimuthal anisotropy and the strike of the Tintina and Denali faults (Fig. 9), as well as a rotation towards absolute plate motion as one crosses eastward towards the the LTZ and the CDF (Snyder & Bruneton, 2007; Courtier et al., 2010; Rasendra et al., 2014; Audet et al., 2016; Bolton et al., 2021). If the lithosphere-asthenosphere boundary to the west of the CDF is only at a depth of 50–60 km (*i.e.,* Audet et al., 2019) then the bulk of the teleseismic shear wave splitting must be accumulated in the as-

thenosphere. This suggests a rotation in asthenospheric flow, from NW-SE near the coast, to NE-SW in the interior. These results were key in developing new tectonic evolution models of the NCC that are described below.

Seismic anisotropy measurements in the Canadian Shield are coherent and roughly parallel to the absolute plate motion direction of the North American plate (Fig. 9), however, fast-axis directions of SKS waves for seismic stations in the Slave craton deviate from it. Snyder and Bruneton (2007) show that SKS splitting measurements and surface waves are best fit by a two-layered mantle beneath the Slave craton. The shallow layer of anisotropy may be associated with a regional tectonic event at 2610-2580 Ma. The deep layer may be partly caused by the present-day absolute plate motion of the north American plate, but also locally to the formation of Kimberlite dykes (Snyder & Bruneton, 2007).

4 Discussion

4.1 Robust features of seismic tomography models of northwestern Canada

We search for common low- and high-velocity anomalies among published seismic tomography models of northwestern Canada by making vote maps (Fig. 10). We choose 3 velocity models for the crust (Kao et al., 2013; Estève et al., 2021; Schutt et al., 2023) and 4 for the uppermost mantle (Estève et al., 2020b; Estève et al., 2021; Schutt et al., 2023). We first define a criterion (see bottom right of each panel in Fig. 10) and search for it at each location within the model space. If this criterion is fulfilled then this location gets a value of 1, if not a value of 0. We repeat this for all seismic tomography models considered and then stack the models. For instance, a value of 4 means that the selected criterion appears at a given location in four different models, thus implying that this feature is robust. Figure 10 shows the resulting maps at 20 (Fig. 10 a-b) and 80 km depths (Fig. 10 c-d). Orange-red colors show robust features from the seismic tomography models considered in this analysis.

At 20 km depth, all three seismic tomography models (*i.e.,* value of 3) show a similar low-velocity anomaly ($\delta V_S < -2\%$) beneath several regions of the NCC: (*i*) the St Elias-Chugach Mountains, (*ii*) between the Tintina and Denali faults, (*iii*) the Mackenzie Mountains, and (*iv*)

in the Yukon Flats of eastern Alaska (Fig. 10a). Common high velocity anomalies ($\delta V_S > 2\%$) highlight the Canadian Shield (Fig. 10b).

At 80 km depth, robust low-velocity anomalies (values of 3 and 4) are observed in the central part of the Mackenzie Mountains, directly east of the Tintina Fault, between the Tintina and the Denali fault and to the north in the Yukon Flats of eastern Alaska (Fig. 10c). High-velocity anomalies are observed in at least 3 models (value of 3) in the Canadian Shield. We note that high-velocity anomalies extend into the NCC in two areas, in the southernmost NCC and in Richardson/northern Mackenzie Mountains (Fig. 10d). The identified robust features are discussed in more details in the following paragraphs.

4.2 Current tectonics

Crustal deformation models of the NCC were developed to explain seismicity and GNSS data that suggest strain/stress transfer and thrusting at the CDF, ∼800 km away from plate boundary forces (Mazzotti & Hyndman, 2002; Hyndman, et al., 2005; Finzel et al., 2014). Seismic velocity models of the crust developed in the last decade (i.e., since deployment of the US-Array TA EarthScope network) confirm that the Moho is broadly flat and shallow across the NCC, with only slight (∼2 km) thickening inferred beneath the MM constrained by sparse data, indicating that there is no Airy-type or otherwise extensive Cordilleran crustal root. This is in contradiction with a satellite gravity gradiometric study (Cadio et al., 2016), which suggests that the topography is perfectly compensated across the NCC interior. In addition, these velocity models suggest that crustal temperatures throughout the NCC are exceptionally high with a Moho temperature reaching 800-900°C (Hyndman, 2017; Audet et al., 2019). The observed low S-wave velocity feature at mid- to lower-crustal depths throughout the NCC (Estève et al., 2021; Schutt et al., 2023) has been interpreted to reflect the elevated temperatures that would buoyantly support high elevations in the absence of a thick crustal root (Lewis et al., 2003; Hyndman & Currie, 2011) (Figs. 3 and 4). The observed low-velocity layer is interpreted by Schutt et al. (2023) as the seismic signature of the lower crustal, rheologically weak layer, described by Mazzotti and Hyndman (2002); Mazzotti et al. (2008), and required to transfer strain from the Yakutat collision zone to the CDF, thus reactivating pre-existing thrust fronts and resulting in the far-field seismicity observed in the Mackenzie Mountains.

Overall, these results favor the thermal isostasy model, where high topographic elevations across the NCC are supported isostatically by uppermost mantle thermal buoyancy due to high temperatures (Lewis et al., 2003; Hasterok et al., 2007; Hyndman & Currie, 2011). Furthermore, such Moho geometry requires that, at some point, the Cordilleran crustal root and associated Moho morphology were flattened out, or removed by thermally activated processes (lower crustal shearing or delamination) during one or several past tectonic events over the entire length of the Canadian Cordillera (*e.g.,* Bao et al., 2014; Chen et al., 2019, in the SCC). Hyndman (2017) suggests that lower crustal flow may have flattened the Moho over a few tens of millions of years. The hypothesis of mantle removal is explored in section 4.4.

Alternatively, Audet et al. (2016) used constraints from SKS splitting data to suggest that the structure of the Proterozoic Laurentian rifted margin may be preserved in the upper mantle (Lund, 2008). According to this model, the LTZ marks the transition from an upper plate margin in the south to a lower plate margin in the north. This is observed as a switch from SW-NE alignment of fast axis of seismic anisotropy coincident with with cratonic lithosphere fabric south of the LTZ, to SE-NW oriented fast axes north of the LTZ. This structure also coincides with the sudden appearance of seismicity north of the LTZ, suggesting that lithospheric mantle tectonic inheritance may partly control seismicity in southeastern NCC (Fig. 9). The buttressing model of Saltus and Hudson (2007) and Estève et al. (2020b) also points to the role of upper mantle strength near the LTZ in controlling the arcuate shape of the CDF in the NCC, with a potential role on Neotectonic activity.

4.3 Beaufort Sea margin

Seismicity and geodetic data suggest that the Beaufort Sea lithosphere is slowly converging ($\sim$2 mm yr^{-1}) with the North American margin, at least between the Canning and Richardson Mountains in northern Yukon, which may lead to or reflect subduction initiation (Hyndman, et al., 2005; Leonard et al., 2007). However, studies on seismicity have historically been limited by the sparse seismic network coverage in this remote region. With the recent availability of seismic data from the EarthScope TA at stations surrounding the Beaufort Sea continental margin, Estève et al. (2022) investigated the structure and deformation of the margin by relocating regional seismicity and developing regional 3-D P-wave, S-wave and V_P/V_S models.

447 P-wave and S-wave velocity models reveal a northwest-dipping low-velocity anomaly through-
448 out the whole crust beneath the Arctic coast of northern Yukon. Interestingly, this low-velocity
449 anomaly is collocated with an area showing no seismicity between November 2012 and August
450 2021 (the earthquake catalogue considered in this study). Based on these observations, the au-
451 thors proposed two scenarios. First, the Beaufort Sea continental margin represents a zone of
452 potential high strain rate, where the lack of seismicity may be indicative of aseismic creep or
453 that strain rates are too low for seismic deformation beneath the Arctic coast of northern Yukon
454 and, thus, current deformation occurs further north offshore within the Beaufort Sea. The au-
455 thors noted that they could not confirm/reject the subduction initiation hypothesis without ad-
456 ditional data from ocean-bottom seismometers deployed in the Beaufort Sea, leaving the ques-
457 tion open.

458 ### 4.4 Mackenzie craton

459 Prior to the TA deployment across Alaska and Yukon, seismic tomography models high-
460 lighted a high-velocity feature west of the CDF beneath northern Yukon (Schaeffer & Lebedev,
461 2014; McLellan et al., 2018) characteristic of cratonic lithosphere. A regional magnetic study
462 identified a long-wavelength magnetic high across northern Yukon that is interpreted as mafic
463 lower crust and underlying depleted upper mantle (Saltus & Hudson, 2007). Schaeffer and Lebe-
464 dev (2014) suggested that this region was underlain by an Archean continental fragment buried
465 beneath the sedimentary strata and that has no surface expression. The high velocity signature
466 of this lithospheric root extends continuously from the Yukon Stable Block underlying central
467 and Northern Yukon, westward through the Mackenzie River Valley and Mackenzie Platform
468 east of the Richardson Mountains; together this lithospheric root is referred to as the Macken-
469 zie craton.

470 Regional seismic tomography models of Alaska and adjacent northwestern Canada also iden-
471 tified a high-velocity feature west of the CDF beneath northern Yukon (Jiang et al., 2018; Feng
472 & Ritzwoller, 2019; Berg et al., 2020). Estève et al. (2020b) further interpreted this relatively
473 high-velocity anomaly within the uppermost mantle as a mechanically-strong and cold lithosphere,
474 supporting the existence of the Mackenzie craton (Figs. 4b-d-f, 7 and 8a-b-g-h, labeled MC). Seis-
475 mic anisotropy measurements (from SKS and $SKKS$ splitting data) across this area are sim-

ilar to those observed across the Canadian Shield, implying that the two regions have preserved similar fabrics, which provides further evidence for the buried Mackenzie craton in northern Yukon (Fig. 9). The presence of the Mackenzie craton in the northern NCC has profound implications for the tectonic evolution of the orogen.

4.5 Cordillera-craton boundary

The arcuate shape and eastward excursion of the NCC is one of the defining features that differentiates it from the SCC. At the surface, the Cordillera-craton boundary is delimited by a sharp topographic change at the CDF that curves westward as one moves north. Such orogenic morphology is often referred to as the result of oroclinal bending, a process that may or may not involve the lithospheric mantle. Understanding this first-order topographic feature is key in constraining the evolution of the NCC. However, prior to the improvements in coverage by new seismograph networks in this region, there were relatively few constraints on the shape of the Cordillera-craton boundary at lower crustal to upper mantle depths.

The first 3-D seismic velocity models suggested that the Cordillera-craton boundary in the upper mantle may be located either at the Tintina Fault (Frederiksen et al., 1998) or at the CDF (Mercier et al., 2009). Subsequent models clearly indicated the presence of cratonic lithosphere underlying the eastern part of the NCC (Schaeffer & Lebedev, 2014; McLellan et al., 2018); thus this boundary was confined to lie somewhere between the Tintina fault and the CDF. In the northernmost NCC, these high seismic velocities west of the CDF are associated with aforementioned Mackenzie craton. Estève et al. (2020b) further proposed that the 3-D structure of the upper mantle plays a key role in controlling the arcuate shape of the NCC through the LTZ and Mackenzie craton acting as rigid buttresses, guiding mantle flow and crustal strain toward the Canadian Shield. This is in agreement with recent geodynamic modeling of the area (McConeghy et al., 2022), as well as the work of Schutt et al. (2023), which shows a zone of lithospheric weakness under the Mackenzie Mountains. The position of the CDF further east within the NCC compared to the SCC may result from weakening of the Proterozoic cratonic lithosphere in the east due to metasomatic modification (Boyce et al., 2023). South of the LTZ, the upper mantle seismic velocity structure of the Proterozoic cratonic lithosphere suggests that it has been preserved

from alteration during the various episodes of deformation that affected the Canadian Cordillera (Boyce et al., 2023).

The absence of thick cratonic lithosphere in the central part of the NCC is enigmatic, as it implies either there never was any thick cratonic lithosphere in the first place, or that this cratonic mantle root was removed. The first clues that point to active removal of lithospheric mantle in the NCC came from Audet et al. (2019), who revealed a west-dipping structure connected to the CDF in the southern NCC. This feature is coincidentally observed as a west-dipping boundary between fast and slow mantle in some seismic velocity models (*e*.g., Schaeffer & Lebedev, 2014), where it places warm asthenospheric mantle overlying a wedge of cold, cratonic lithosphere. This unexpected "oro-ward" dipping boundary in the upper mantle is also resolved by magnetotelluric data and seismic velocity models in the southernmost SCC (*e.g.,* Rippe et al., 2013; Chen et al., 2019). It remains unclear whether these structures reflect the remnant of a mantle suture zone (*e.g.,* Chen et al., 2019; Audet et al., 2019) or represent a transient feature associated with gravitational instability, thermal erosion and mantle-flow driven stresses from a sub-vertical boundary in lithospheric thickness (*e.g.,* Eaton et al., 2018; Yu et al., 2022; Currie et al., 2023). Given the numerous configurations of the Cordillera-craton boundary observed spanning the Canadian Cordillera as a whole, we suggest that mapping this boundary at upper mantle depth is a primary target for future investigations.

4.6 Tintina Fault

The Tintina Fault is a major tectonic structure spanning the NCC that has accommodated more than 400 km of horizontal displacement between Late Cretaceous and Eocene time (Gabrielse et al., 2006; Hayward, 2015). Imaging the structure of the Tintina Fault was one of the objectives of the Lithoprobe SNORCLE experiment. Controlled-source seismic and magnetotelluric data suggested that the Tintina Fault is a crustal-scale feature (Cook & Erdmer, 2005; Dehkordi et al., 2019). Estève et al. (2020a) investigated the vertical extent of the Tintina Fault and its role in the tectonic evolution of the NCC by combining seismic observations from seismic anisotropy measurements and tomographic images of the upper mantle. They reported strong seismic velocity contrasts across the Tintina Fault associated with the progressive clockwise rotation of fast-axis directions and increasing delay times along most of its length. Such seismic velocity

contrasts cannot be related to a thermal anomaly, as the Tintina Fault was last active in the Eocene. Instead, they proposed that the Tintina Fault is a trans-lithospheric fault bounding lithospheric mantle regions with distinct compositions. This is further supported by an estimated 2 % increase in P-wave velocity between NCC and Greenland (cratonic) xenoliths (see Supplemental material of Estève et al., 2020a).This interpretation brings into question the thrust-sheet model of terrane accretion over a Precambrian basement suggested by the SNORCLE data. Instead, these results indicate large-scale displacement of lithospheric material over several hundred kilometers between Late Cretaceous and the Eocene. In particular, two inferred cratonic fragments are thought to have been chiseled and displaced along the Tintina Fault (Fig. 8 a-b, labeled F1 and F2). Those cratonic fragments are associated with the Cassiar terrane in the southern area of the NCC and a remnant of the Mackenzie craton in eastern Alaska, USA.

To complement the teleseismic body-wave tomography model of Estève et al. (2020b), Estève et al. (2021) and Schutt et al. (2023) used surface-wave tomography and investigated the structure of the crust and the top 50 km of the uppermost mantle. The shallow uppermost mantle S-wave velocity structure (50–100 km depth) is consistent with the deeper uppermost mantle seismic velocity structure obtained from teleseismic body-wave tomography. The S-wave velocity model shows a vertical low-velocity region bounded by sharp S-wave velocity gradients occurring beneath the surface expression of the Denali and Tintina faults (Fig. 4d). Moreover, the overlying crust is thinner directly above this low-velocity region in the uppermost mantle. Interestingly, a similar low-velocity anomaly is present in the teleseismic body-wave tomography models of Estève et al. (2020b) and extends down to 500 km depth, but the authors loosely interpreted it in terms of compositional variations in the mantle (Fig. 8 g-h). Based on their velocity model and additional geological evidence, Estève et al. (2021) proposed that this low-velocity region in the uppermost mantle may represent the upwelling of deeper and hotter asthenospheric material caused by the 430 km of lithospheric-scale dextral motion along the Tintina Fault between the Late Cretaceous and the Eocene. Furthermore, this unusually hot region within the uppermost mantle may have thinned the base of the overlying crust through thermal erosion. Notably, these uppermost mantle velocity variations suggest a non-uniform temperature distribution in the mantle lithosphere, and a variable lithospheric thickness.

5 Conclusions and Perspective

The EarthScope USArray TA deployment, in combination with other seismological networks, has provided an unprecedented high-resolution seismic data set of Alaska and northwestern Canada in an area that until recently has been poorly instrumented. This data set enables addressing fundamental questions on current geodynamics and the tectonic evolution of the NCC. Numerous geophysical studies benefited from this data set and the results obtained have provided new insights regarding the structure, origin and deformation of the lithosphere in the NCC, for instance:

- Seismic tomography models revealed that the lower crust beneath the NCC is anomalously slow from the Yakutat collision zone to the CDF (Estève et al., 2021; Schutt et al., 2023). Such low seismic velocities reflect the widespread elevated temperatures across the Cordillera (temperatures at the Moho reach 800-900° C) and could also reflect the strain transfer from the Yakutat collision zone to the Mackenzie Mountains, described by Mazzotti and Hyndman (2002).
- The seismic velocity structure beneath the currently uplifting Mackenzie Mountains is marked by a large low-velocity anomaly extending from the upper crust into the uppermost mantle, which is interpreted as a transcrustal elevated temperature anomaly (Schutt et al., 2023). However, there are no signs of recent magmatism nor volcanism in this area. Future work should focus on identifying the nature and magnitude of the low-velocity anomaly underlying the Mackenzie Mountains. Deployment of magnetotelluric instruments in the region would provide complementary information to the currently available seismic data sets, and additional seismometers would better constrain the location of the anomaly.
- Seismic data and models support the notion that variations in mantle lithospheric strength control current mantle flow conditions and surface deformation in the NCC (Estève et al., 2020b; Estève et al., 2021; Schutt et al., 2023; Boyce et al., 2023). For instance, the LTZ in the southern NCC marks a lithospheric-scale boundary inherited from the Proterozoic rifting of Laurentia that may be controlling neotectonic activity in this region. Combined with the inferred cratonic root of the Mackenzie craton in the northern NCC, these thick and rigid lithospheric blocks may further control the arcuate morphology of the NCC through buttressing of the mantle flow.

- Lastly, seismic tomography models and seismic anisotropy measurements strongly suggest that the Tintina Fault penetrates into the lithospheric mantle and displaced cratonic fragments to the northwest over several hundreds of kilometers between late Cretaceous and the Eocene (Estève et al., 2020a), placing new constraints on plate reconstructions.

Future efforts should focus on refining estimates of the lithospheric thickness and the mantle transition zone throughout the NCC (e.g., using S-to-P receiver function analysis), as this will provide constraints on the development and stability of lithospheric plates. In addition, the crustal and upper mantle seismic attenuation structure of the NCC should be investigated, as this is a powerful tool that is sensitive to temperature variations and to the presence of melt, but less sensitive to composition when compared to seismic velocities (Dalton et al., 2009). It would be useful to convert the seismic velocity variations into temperature and viscosity, and geodynamically model these, to better understand how such variations control the location of orogenesis. Additionally, large velocity variations in the upper mantle to the west of the CDF suggest a complicated lithospheric structure, that may be caused by a delaminating lithosphere.

Acknowledgments

The authors thank two anonymous reviewers for their comments that helped improve this paper. The authors also thank the various federal, territorial, and municipal agencies in the Yukon and Northwest Territories (Government of Yukon Highways and Public Works, Government of Yukon Energy Mines and Resources, towns of Faro and Norman Wells, British Columbia Wildfire Service, Northwest Territories Environment and Natural Resources, and NAV CANADA) for allowing the authors access to their land in the installation of the Yukon–Northwest Seismograph Network. This research regards the ancestral homelands of hundreds of diverse and distinct Indigenous Peoples. PA acknowledges and respects that his workplace stands on unceded Algonquin territory. This project was supported by the Canadian Foundation for Innovation (30318), the Natural Science and Engineering Research Council of Canada (Discovery Grant RGPIN-2018-03752), the NSF EarthScope awards 1460536 and 1460533, and FRES award 1925595. The facilities of IRIS Data Services, and specifically the IRIS Data Management Center, were used to access waveforms, metadata, and data products used in the studies. IRIS Data Services are funded

through the Seismological Facilities for the Advancement of Geoscience and EarthScope (SAGE) Proposal of the National Science Foundation under Cooperative Agreement EAR-1851048.

Data Availability Statement

The facilities of IRIS Data Services, and specifically the IRIS Data Management Center, were used for archiving and access to waveforms, related metadata, and/or derived products used in this study. IRIS Data Services are funded through the Seismological Facilities for the Advancement of Geoscience and EarthScope (SAGE) Proposal of the National Science Foundation under Cooperative Agreement EAR-1261681. Data from the TA network were made freely available as part of the EarthScope USArray facility, operated by Incorporated Research Institutions for Seismology (IRIS) and supported by the National Science Foundation, under Cooperative Agreements EAR-1261681. Data are available on the IRIS Earthquake Data Center (https://ds.iris.edu/ds/nodes/dm The seismic models were directly provided by the corresponding authors. Figures were created using Generic Mapping Tools (Wessel et al., 2013). Figure 10 was created using the Geophysical Model Generator (https://github.com/JuliaGeodynamics/GeophysicalModelGenerator.jl) and Paraview (Ahrens et al., 2005).

References

Ahrens, J. P., Geveci, B., & Law, C. C. (2005). ParaView: An End-User Tool for Large-Data Visualization. *The Visualization Handbook*.

Aster, R. C., & Shearer, P. M. (1992). Initial shear-wave particle motions and stress constraints at the anza seismic network. *Geophysical Journal International*, *108*(3), 740-748.

Audet, P., Currie, C. A., Schaeffer, A. J., & Hill, A. M. (2019). Seismic evidence for lithospheric thinning and heat in the Northern Canadian Cordillera. *Geophysical Research Letters*, *46*, 1–9. doi: https://doi.org/10.1029/2019GL082406

Audet, P., Jellinek, A. M., & Uno, H. (2007). Mechanical controls on the deformation of continents at convergent margins. *Earth and Planetary Science Letters*, *264*(1-2), 151–166. doi: https://doi.org/10.1016/j.epsl.2007.09.024

Audet, P., Schutt, D. L., Schaeffer, A. J., Estève, C., Aster, R. C., & Cubley, J. F. (2020). Moho variations across the northern Canadian Cordillera. *Seismological Research Letters*, *91*(6), 3076–3085. doi: https://doi.org/10.1785/0220200166

Audet, P., Sole, C., & Schaeffer, A. J. (2016). Control of lithospheric inheritance on neotectonic activity in northwestern Canada? *Geology*, *44*(10), 807–810. doi: https://doi.org/10.1130/G38118.1

Baker, M. G., Heath, D. C., Derek, L., Aster, R. C., Cubley, J. F., & Freymueller, T. (2019). The Mackenzie Mountains EarthScope Project: Studying Active Deformation in the Northern North American Cordillera from Margin to Craton. *Seismological Research Letters*, 1–12. doi: https://doi.org/10.1785/0220190139

Bao, X., Eaton, D. W., & Guest, B. (2014). Plateau uplift in western Canada caused by lithospheric delamination along a craton edge. *Nature Geoscience*, *7*(11), 830–833. doi: https://doi.org/10.1038/ngeo2270

Becker, T. W., & Lebedev, S. (2021). Dynamics of the upper mantle in light of seismic anisotropy. In *Mantle convection and surface expressions* (p. 257-282). American Geophysical Union (AGU). doi: https://doi.org/10.1002/9781119528609.ch10

Bedle, H., & van der Lee, S. (2009). S velocity variations beneath North America. *Journal of Geophysical Research*, *114*, 1–22. doi: https://doi.org/10.1029/2008JB005949

Berg, E. M., Lin, F. C., Allam, A., Schulte-Pelkum, V., Ward, K. M., & Shen, W. (2020). Shear Velocity Model of Alaska Via Joint Inversion of Rayleigh Wave Ellipticity, Phase Velocities, and Receiver Functions Across the Alaska Transportable Array. *Journal of Geophysical Research: Solid Earth*, *125*(2), 1–22. doi: https://doi.org/10.1029/2019JB018582

Bolton, A. R., Schutt, D. L., Aster, R. C., Audet, P., Schaeffer, A. J., Estève, C., ... Cubley, J. F. (2021). Evidence for asthenospheric flow rotation in northwest canada: insights from shear wave splitting. *Geophysical Journal International*, *228*(3), 1780–1792. doi: https://doi.org/10.1093/gji/ggab396

Boyce, A., Liddell, M., Pugh, S., Brown, J., McMurchie, E., Parsons, A., ... Aster, R. (2023). A new P-wave Tomographic model (CAP22) for North America: implications for the subduction and cratonic metasomatic modification history of western Canada and Alaska. *Jounal of Geophysical Research: Solid Earth*, *128*, e2022JB025745. doi: https://doi.org/10.1029/2022JB025745

Buchbinder, G. G. R., & Poupinet, G. (1977). P-wave residuals in Canada. *Canadian Journal of Earth Sciences*, *14*, 1292–1304. doi: https://doi.org/10.1139/e77-118

Busby, R. W., & Aderhold, K. (2020). The Alaska Transportable Array: As Built. *Seismological Research Letters*, *91*(6), 3017-3027. doi: https://doi.org/10.1785/0220200154

Cadio, C., Saraswati A., Cattin R., & Mazzotti S. (2016). A new approach to assess isostatic compensation of topography in continental domain from GOCE gravity gradients. *Geophysical Journal International*, *207*(2), 645-654. doi: https://doi.org/10.1093/gji/ggw281

Cassidy, J. F., Rogers G. C., & Ristau J. W. (2005). Seismicity in the vicinity of the SNORCLE corridors of the northern Canadian Cordillera. *Canadian Journal of Earth Sciences*, *42*(6), 1137-1148. doi: https://doi.org/10.1139/e04-063

Chen, Y., Gu, Y. J., Currie, C. A., Johnston, S. T., Shu-Huei, H., Schaeffer, A. J., & Audet, P. (2019). Seismic evidence for a mantle suture and implications for the origin of the Canadian Cordillera. *Nature Communications*, 1–10. doi: https://doi.org/10.1038/s41467-019-09804-8

Clowes, R. M., Hammer, P. T., Fernández-Viejo, G., & Welford, J. K. (2005, 09). Lithospheric structure in northwestern Canada from Lithoprobe seismic refraction and

related studies: a synthesis1,2. *Canadian Journal of Earth Sciences*, *42*(6), 1277-1293. doi: https://doi.org/10.1139/e04-069

Colpron, M., Nelson, J. A. L., & Murphy, D. C. (2007). Northern Cordilleran terranes and their interactions through time. *GSA Today*, *17*(4-5), 4–10. doi: https://doi.org/10.1130/GSAT01704-5A.1

Cook, F. A. (2002, 01). Fine structure of the continental reflection Moho. *GSA Bulletin*, *114*(1), 64-79. doi: https://doi.org/10.1130/0016-7606(2002)114<0064:FSOTCR>2.0.CO;2

Cook, F. A., & Erdmer, P. (2005). An 1800 km cross section of the lithosphere through the northwestern North American plate: lessons from 4.0 billion years of Earth's history. *Canadian Journal of Earth Sciences*, *42*, 1295–1311. doi: https://doi.org/10.1139/e04-106

Courtier, A. M., Gaherty, J. B., Revenaugh, J., Bostock, M. G., & Garnero, E. J. (2010). Seismic anisotropy associated with continental lithosphere accretion beneath the CANOE array, Northwestern Canada. *Geology*, *38*(10), 887–890. doi: https://doi.org/10.1130/G31120.1

Currie, C. A., Huismans, R. S., & Beaumont, C. (2008). Thinning of continental backarc lithosphere by flow-induced gravitational instability. *Earth and Planetary Science Letters*, *269*(3), 436-447. doi: https://doi.org/10.1016/j.epsl.2008.02.037

Currie, C. A., Mallyon, D. A., Yu, T.-C., Chen, Y., Schaeffer, A. J., Audet, P., & Gu, Y. J. (2023). Mantle structure and dynamics at the eastern boundary of the northern Cascadia backarc. *Journal of Geodynamics*, *155*, 101958. doi: https://doi.org/10.1016/j.jog.2022.101958

Dalton, C. A., Ekström, G., & Dziewonski, A. M. (2009). Global seismological shear velocity and attenuation: A comparison with experimental observations. *Earth and Planetary Science Letters*, *284*(1), 65-75. doi: https://doi.org/10.1016/j.epsl.2009.04.009

Dalton, C. A., Gaherty, J. B., & Courtier, A. M. (2011). Crustal VS structure in northwestern Canada : Imaging the Cordillera - craton transition with ambient noise tomography. *Journal of Geophysical Research*, *116*, 1–30. doi: https://doi.org/10.1029/2011JB008499

Dehkordi, B. H., Ferguson, I. J., Jones, A. G., Ledo, J., & Wennberg, G. (2019). Tectonics

of the northern Canadian Cordillera imaged using modern magnetotelluric analysis. *Tectonophysics*, *765*, 102–128. doi: https://doi.org/10.1016/j.tecto.2019.05.012

DeMets, C., Gordon, R. G., & Argus, D. F. (2010). Geologically current plate motions. *Journal of Geodynamics*, *100*, 144–158. doi: https://doi.org/10.1016/j.jog.2016.03.015

Eaton, D. W., Bao, X., & Perry, C. (2018). Frayed edges of cratonic mantle keels. In *Lithospheric discontinuities* (p. 125-138). American Geophysical Union (AGU). doi: https://doi.org/10.1002/9781119249740.ch7

Estève, C., Audet, P., Schaeffer, A. J., Schutt, D., Aster, R. C., & Cubley, J. (2020b). The upper mantle structure of northwestern Canada from teleseismic body wave tomography. *Journal of Geophysical Research: Solid Earth*, *125*, 1–18. doi: https://doi.org/10.1029/2019JB018837

Estève, C., Audet, P., Schaeffer, A. J., Schutt, D. L., Aster, R. C., & Cubley, J. F. (2020a). Seismic evidence for craton chiseling and displacement of lithospheric mantle by the Tintina fault in the northern Canadian Cordillera. *Geology*, *48*. doi: https://doi.org/10.1130/g47688.1

Estève, C., Gosselin, J., Audet, P., Schaeffer, A., Schutt, D., & Aster, R. (2021). Surface wave tomography of the northern Canadian Cordillera using earthquake Rayleigh wave group velocities. *Journal of Geophysical Research: Solid Earth*, *126*(8), e2021JB02196. doi: https://doi.org/10.1029/2021JB021960

Estève, C., Liu, Y., Koulakov, I., Schaeffer, A. J., & Audet, P. (2022). Seismic Evidence for a Weakened Thick Crust at the Beaufort Sea Continental Margin. *Geophysical Research Letters*, *49*(16). doi: https://doi.org/10.1029/2022GL100158

Estève, C., Schaeffer, A. J., & Audet, P. (2019). Upper mantle structure underlying the diamondiferous slave craton from teleseismic body-wave tomography. *Tectonophysics*, *757*, 187-202. doi: https://doi.org/10.1016/j.tecto.2019.01.012

Feng, L., & Ritzwoller, M. H. (2019). A 3-d shear velocity model of the crust and uppermost mantle beneath Alaska including apparent radial anisotropy. *Journal of Geophysical Research: Solid Earth*, *124*(10), 10468-10497. doi: https://doi.org/10.1029/2019JB018122

Finzel, E. S., Flesch, L. M., & Ridgway, K. D. (2014). Present-day geodynamics of the

northern North American Cordillera. *Earth and Planetary Science Letters*, *404*, 111–123. doi: https://doi.org/10.1016/j.epsl.2014.07.024

Finzel, E. S., Flesch, L. M., Ridgway, K. D., Holt, W. E., & Ghosh, A. (2015). Surface motions and intraplate continental deformation in alaska driven by mantle flow. *Geophysical Research Letters*, *42*(11), 4350-4358. doi: https://doi.org/10.1002/2015GL063987

Flück, P., Hyndman, R. D., & Lowe, C. (2003). Effective elastic thickness T e of the lithosphere in western Canada. *Journal of Geophysical Research*, *108*(B9), 15. doi: https://doi.org/10.1029/2002jb002201

Frederiksen, A. W., Bostock, M. G., & Cassidy, J. F. (2001). S-wave velocity structure of the Canadian upper mantle. *Physics of the Earth and Planetary Interiors*, *124*(3-4), 175–191. doi: https://doi.org/10.1016/S0031-9201(01)00194-7

Frederiksen, A. W., Bostock, M. G., VanDecar, J. C., & Cassidy, J. F. (1998). Seismic structure of the upper mantle beneath the northern Canadian Cordillera from teleseismic travel-time inversion. *Tectonophysics*, *294*(1-2), 43–55. doi: https://doi.org/10.1016/S0040-1951(98)00095-X

Gabrielse, H., Murphy, D. C., & Mortensen, J. K. (2006). Cretaceous and Cenozoic dextral orogen-parallel displacements, magmatism, and paleogeography, north-central Canadian Cordillera. In J. W. H. Haggart, J. W., Enkin, R. J. and Monger (Ed.), *Paleogeography of the North American Cordillera: Evidence For and Against Large-Scale Displacements: Geological Association of Canada* (pp. 255–276).

Gabrielse, H., & Yorath, C. (1991). *Geology of the Cordilleran Orogen in Canada*. Geological Society of America. doi: 10.1130/DNAG-GNA-G2

Gaudreau, E., Audet, P., & Schneider, D. A. (2019). Mapping Curie Depth Across Western Canada From a Wavelet Analysis of Magnetic Anomaly Data. *Journal of Geophysical Research: Solid Earth*, *124*, 1–21. doi: https://doi.org/10.1029/2018JB016726

Gosselin, J. M., Audet, P., Schaeffer, A. J., Darbyshire, F. A., & Estève, C. (2021). Azimuthal anisotropy in Bayesian surface wave tomography: application to northern Cascadia and Haida Gwaii, British Columbia. *Geophysical Journal International*, *224*(3), 1724-1741. doi: https://doi.org/10.1093/gji/ggaa561

Grand, S. P. (1994). Mantle shear structure beneath the americas and surrounding oceans.

Journal of Geophysical Research: Solid Earth, *99*(B6), 11591-11621. doi: https://doi.org/10.1029/94JB00042

Hansen, L. N., Faccenda, M., & Warren, J. M. (2021). A review of mechanisms generating seismic anisotropy in the upper mantle. *Physics of the Earth and Planetary Interiors*, *313*, 106662. doi: https://doi.org/10.1016/j.pepi.2021.106662

Hasterok, D., & Chapman, D. S. (2007). Continental thermal isostasy: 2. Application to North America. *Journal of Geophysical Research: Solid Earth*, *112*, B06415. doi: https://doi.org/10.1029/2006JB004664

Hayward, N. (2015). Geophysical investigation and reconstruction of lithospheric structure and its control on geology, structure, and mineralization in the Cordillera of northern Canada and eastern Alaska. *Tectonics*, *34*(10), 2165–2189. doi: https://doi.org/10.1002/2015TC003871

Hyndman, R. D. (2017). Lower-crustal flow and detachment in the North American Cordillera: a consequence of Cordillera-wide high temperatures. *Geophysical Journal International*, *209*(3), 1779–1799. doi: https://doi.org/10.1093/gji/ggx138

Hyndman, R. D., & Currie, C. A. (2011). Why is the North America Cordillera high? Hot backarcs, thermal isostasy, and mountain belts. *Geology*, *39*(8), 783–786. doi: https://doi.org/10.1130/G31998.1

Hyndman, R. D., Currie, C. A., & Mazzotti, S. (2005). Subduction zone backarcs, mobile belts, and orogenic heat. *GSA Today*, *15*(2), 4–10. doi: https://doi.org/10.1130/1052-5173(2005)015

Hyndman, R. D., Flück, P., Mazzotti, S., Lewis, T. J., Ristau, J., & Leonard, L. J. (2005). Current tectonics of the northern Canadian Cordillera. *Canadian Journal of Earth Sciences*, *42*(6), 1117–1136. doi: https://doi.org/10.1139/e05-023

Jiang, C., Schmandt, B., Ward, K. M., Lin, F. C., & Worthington, L. L. (2018). Upper Mantle Seismic Structure of Alaska From Rayleigh and S Wave Tomography. *Geophysical Research Letters*, *45*, 10350–10359. doi: https://doi.org/10.1029/2018GL079406

Johnston, S. T. (2008). The Cordilleran Ribbon Continent of North America. *Annual Review of Earth and Planetary Sciences*, *36*, 495–530. doi: https://doi.org/10.1146/annurev.earth.36.031207.124331

Jones, A. G., Ledo, J., Ferguson, I. J., Farquharson, C., Garcia, X., Grant, N., ... Wu, X. (2005). The electrical resistivity structure of Archean to Tertiary lithosphere along 3200 km of SNORCLE profiles, northwestern Canada. *Canadian Journal of Earth Sciences*, *42*(6), 1257–1275. doi: https://doi.org/10.1139/e05-080

Kao, H., Behr, Y., Currie, C. A., Hyndman, R. D., Townend, J., Lin, F. C., ... He, J. (2013). Ambient seismic noise tomography of Canada and adjacent regions: Part I. Crustal structures. *Journal of Geophysical Research: Solid Earth*, *118*(11), 5865–5887. doi: https://doi.org/10.1002/2013JB010535

Kennett, B. L. N., Engdahl, E. R., & Buland, R. (1995). Constraints on seismic velocities in the Earth from traveltimes. *Geophysical Journal International*, *122*(1), 108–124. doi: https://doi.org/10.1111/j.1365-246X.1995.tb03540.x

Ledo, J., Jones, A. G., & Ferguson, I. J. (2002). Electromagnetic images of a strike-slip fault: The Tintina fault-Northern Canadian. *Geophysical Research Letters*, *29*(8), 1–4. doi: https://doi.org/10.1029/2001gl013408

Leonard, L. J., Hyndman, R. D., Mazzotti, S., Nykolaishen, L., Schmidt, M., & Hippchen, S. (2007). Current deformation in the northern Canadian Cordillera inferred from GPS measurements. *Journal of Geophysical Research: Solid Earth*, *112*(11), 1–15. doi: https://doi.org/10.1029/2007JB005061

Lewis, T. J., Hyndman, R. D., & Fluck, P. (2003). Heat flow, heat generation, and crustal temperatures in the northern Canadian Cordillera: Thermal control of tectonics. *Journal of Geophysical Research-Solid Earth*, *108*(B6), 18. doi: https://doi.org/10.1029/2002JB002090

Lowe, C., & Cassidy, J. F. (1995). Geophysical evidence for crustal thickness variations between the denali and tintina fault systems in west-central yukon. *Tectonics*, *14*(4), 909-917. doi: https://doi.org/10.1029/95TC00087

Lund, K. (2008). Geometry of the Neoproterozoic and Paleozoic rift margin of western Laurentia: Implications for mineral deposit settings. *Geological Society of America Geosphere*, *4*(2), 429–444. doi: https://doi.org/10.1130/GES00121.1

Mazzotti, S., & Hyndman, R. D. (2002). Yakutat collision and strain transfer across the northern Canadian Cordillera. *Geology*, *30*(6), 495–498. doi: https://doi.org/10.1130/0091-7613(2002)030<0495:YCASTA>2.0.CO;2

Mazzotti, S., Leonard, L. J., Hyndman, R. D., & Cassidy, J. F. (2008). Tectonics , Dynamics , and Seismic Hazard in the Canada – Alaska Cordillera. *Active Tectonics and Seismic Potential of Alaska*, 297–319.

McConeghy, J., Flesch, L., & Elliott, J. (2022). Investigating the Effect of Mantle Flow and Viscosity Structure on Surface Velocities in Alaska Using 3-D Geodynamic Models. *Journal of Geophysical Research: Solid Earth*, 1–24. doi: https://doi.org/10.1029/2022jb024704

McLellan, M., Schaeffer, A. J., & Audet, P. (2018). Structure and fabric of the crust and uppermost mantle in the northern Canadian Cordillera from Rayleigh-wave tomography. *Tectonophysics*, *724-725*, 28–41. doi: https://doi.org/10.1016/j.tecto.2018.01.011

Meier, T., Dietrich, K., Stöckhert, B., & Harjes, H.-P. (2004). One-dimensional models of shear wave velocity for the eastern Mediterranean obtained from the inversion of Rayleigh wave phase velocities and tectonic implications. *Geophysical Journal International*, *156*(1), 45-58. doi: https://doi.org/10.1111/j.1365-246X.2004.02121.x

Mercier, J. P., Bostock, M. G., Cassidy, J. F., Dueker, K., Gaherty, J. B., Garnero, E. J., ... Zandt, G. (2009). Body-wave tomography of western Canada. *Tectonophysics*, *475*(3-4), 480–492. doi: https://doi.org/10.1016/j.tecto.2009.05.030

Miller, M., Driscoll, L. J. O., Porritt, R. W., & Roeske, S. M. (2018). Multiscale crustal architecture of Alaska inferred from P receiver functions. *Geological Society of America*, *10*(2), 267–278. doi: https://doi.org/10.1130/L701.1

Nelson, J. L., Colpron, M., & Israel, S. (2013). The Cordillera of British Columbia , Yukon , and Alaska : Tectonics and Metallogeny. *Society of Economic Geologists*, *17*, 53–109. doi: https://doi.org/10.5382/SP.17

Oldow, J. S., Bally, A. W., & Ave Lallemant, H. G. (1990). Transpression, orogenic float, and lithospheric balance. *Geology*, *18*(10), 991–994. doi: https://doi.org/10.1130/0091-7613(1990)018<0991:TOFALB>2.3.CO

Park, J., & Levin, V. (2002). Seismic anisotropy: Tracing plate dynamics in the mantle. *Science*, *296*(5567), 485-489. doi: https://doi.org/10.1126/science.1067319

Perry, H. K. C., Eaton, D. W. S., & Forte, A. M. (2002, 07). LITH5.0: a revised crustal model for Canada based on Lithoprobe results. *Geophysical Journal International*,

150(1), 285-294. Retrieved from https://doi.org/10.1046/j.1365-246X.2002.01712.x doi: 10.1046/j.1365-246X.2002.01712.x

Postlethwaite, B., Bostock, M. G., Christensen, N. I., & Snyder, D. B. (2014). Seismic velocities and composition of the Canadian crust. *Tectonophysics*, *633*(1), 256–267. doi: https://doi.org/10.1016/j.tecto.2014.07.024

Rasendra, N., Bonnin, M., Mazzotti, S., & Tiberi, C. (2014). Crustal and upper-mantle anisotropy related to fossilized transpression fabric along the denali fault, Northern Canadian Cordillera. *Bulletin of the Seismological Society of America*, *104*(4), 1964–1975. doi: https://doi.org/10.1785/0120130233

Rippe, D., Unsworth, M. J., & Currie, C. A. (2013). Magnetotelluric constraints on the fluid content in the upper mantle beneath the southern canadian cordillera: Implications for rheology. *Journal of Geophysical Research: Solid Earth*, *118*(10), 5601-5624. doi: https://doi.org/10.1002/jgrb.50255

Ristau, J., Rogers G. C., & Cassidy J. F. (2007). Stress in western Canada from regional moment tensor analysis. *Canadian Journal of Earth Sciences*, *44*(2), 127-148. doi: https://doi.org/10.1139/e06-057

Saltus, R. W., & Hudson, T. L. (2007). Regional magnetic anomalies , crustal strength , and the location of the northern Cordilleran fold-and-thrust belt. *The Geological Society of America*, *35*(6), 567–570. doi: https://doi.org/10.1130/G23470A.1

Savage, M. K. (1999). Seismic anisotropy and mantle deformation: what have we learnt from shear wave splitting? *Reviews of Geophysics*, *37*(1), 65–106. doi: https://doi.org/10.1029/98RG02075

Schaeffer, A. J., & Lebedev, S. (2014). Imaging the North American continent using waveform inversion of global and USArray data. *Earth and Planetary Science Letters*, *402*(C), 26–41. doi: https://doi.org/10.1016/j.epsl.2014.05.014

Schmandt, B., & Lin, F.-C. (2014). P and S wave tomography of the mantle beneath the united states. *Geophysical Research Letters*, *41*(18), 6342–6349. doi: https://doi.org/10.1002/2014GL061231

Schutt, D. L., Porritt, R. W., Estève, C., Audet, P., Gosselin, J. M., Schaeffer, A. J., ... Cubley, J. F. (2023). Lithospheric S wave velocity variations beneath the Mackenzie Mountains and Northern Canadian Cordillera. *Journal of Geophysical Research: Solid*

Earth, *128*(1), e2022JB025517. doi: https://doi.org/10.1029/2022JB025517

Snyder, D. B., & Bruneton, M. (2007). Seismic anisotropy of the Slave craton, NW Canada, from joint interpretation of SKS and Rayleigh waves. *Geophysical Journal International*, *169*(1), 170–188. doi: https://doi.org/10.1111/j.1365-246X.2006.03287.x

Snyder, D. B., Clowes, R. M., Cook, F. A., Erdmer, P., Evenchick, C. A., van der Velden, A. J., & Hall, K. W. (2002). Proterozoic prism arrests suspect terranes: Insights into the ancient Cordilleran margin from seismic reflection data. *GSA Today*, *12*, 4–10. doi: https://doi.org/10.1130/1052-5173(2002)012<0004:PPASTI>2.0.CO;2

Tarayoun, A., Audet, P., Mazzotti, S., & Ashoori, A. (2017). Architecture of the crust and uppermost mantle in the northern Canadian Cordillera from receiver functions. *Journal of Geophysical Research: Solid Earth*, *122*(7), 5268–5287. doi: https://doi.org/10.1002/2017JB014284

Thorkelson, D. J., Madsen, J. K., & Sluggett, C. L. (2011). Mantle flow through the Northern Cordilleran slab window revealed by volcanic geochemistry. *Geology*, *39*(3), 267–270. doi: https://doi.org/10.1130/G31522.1

van der Lee, S., & Frederiksen, A. W. (2005). Surface wave tomography applied to the North American upper mantle. *Seismic Earth: ArrayAnalysis of Broadband Seismograms, Geophys. Monogr. Ser.*, *157*, 67–80. doi: https://doi.org/10.1029/157GM05

Venereau, C. M. A., Martin-Short, R., Bastow, I. D., Allen, R. M., & Kounoudis, R. (2019). The role of variable slab dip in driving mantle flow at the eastern edge of the Alaskan subduction margin: insights from shear-wave splitting. *Geochemistry, Geophysics, Geosystems*, *20*, 2433–2448. doi: https://doi.org/10.1029/2018gc008170

Ward, K. M. (2015). Ambient noise tomography across the southern Alaskan Cordillera. *Geophysical Research Letters*, *42*, 3218–3227. doi: https://doi.org/10.1002/2015GL063613.Received

Wessel, P., Smith, W. H. F., Scharroo, R., Luis, J., & Wobbe, F. (2013). Generic mapping tools: Improved version released. *Eos*, *94*(45), 409–410. doi: https://doi.org/10.1002/2013EO450001

Wickens, A. J. (1977). The upper mantle of southern British Columbia. *Canadian Journal of Earth Sciences*, *14*(5), 1100–1115. doi: https://doi.org/10.1139/e77-101

Wickens, A. J., & Buchbinder, G. G. R. (1980). S-wave residuals in Canada. *Bulletin*

of the Seismological Society of America, *70*(3), 809–822. doi: https://doi.org/10.1785/BSSA0700030809

Yu, T.-C., Currie, C. A., Unsworth, M. J., & Chase, B. F. W. (2022). The structure and dynamics of the uppermost mantle of southwestern canada from a joint analysis of geophysical observations. *Journal of Geophysical Research: Solid Earth*, *127*(10), e2022JB024130. doi: https://doi.org/10.1029/2022JB024130

Zaporozan, T., Frederiksen, A. W., Bryksin, A., & Darbyshire, F. A. (2018). Surface-wave images of western Canada: lithospheric variations across the Cordillera–craton boundary. *Canadian Journal of Earth Sciences*, *10*(999), 1–10. doi: https://doi.org/10.1139/cjes-2017-0277

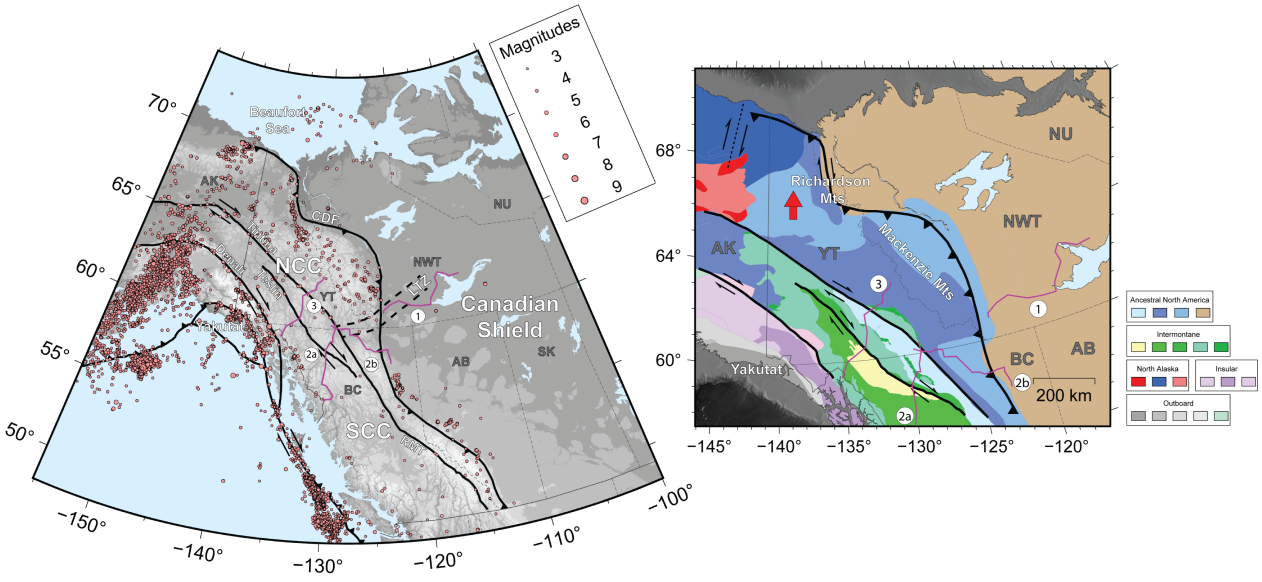

Figure 1. (a) Topographic map of western Canada and eastern Alaska. Red dots represent seismicity ($M_W \geq 3.0$) between 2012 and 2022 from the USGS and nrCAN catalogs. Purple lines denote the 3 Lithoprobe SNORCLE profiles across northwestern Canada. The dashed-line shows the Canning River deformation zone. (b) Terrane map of northwestern Canada and eastern Alaska. Single red arrow shows northward residual motion. Abbreviations: AB, Alberta; AK, Alaska; BC, British Columbia; CDF, Cordillera Deformation Front; LTZ, Liard Transfer Zone; NCC, Northern Canadian Cordillera; NU, Nunavut; NWT, Northwest Territories; SCC, Southern Canadian Cordillera; SK, Saskatchewan; RMT, Rocky Mountain Trench; YT, Yukon Territory. Terranes adapted from Colpron et al. (2007).

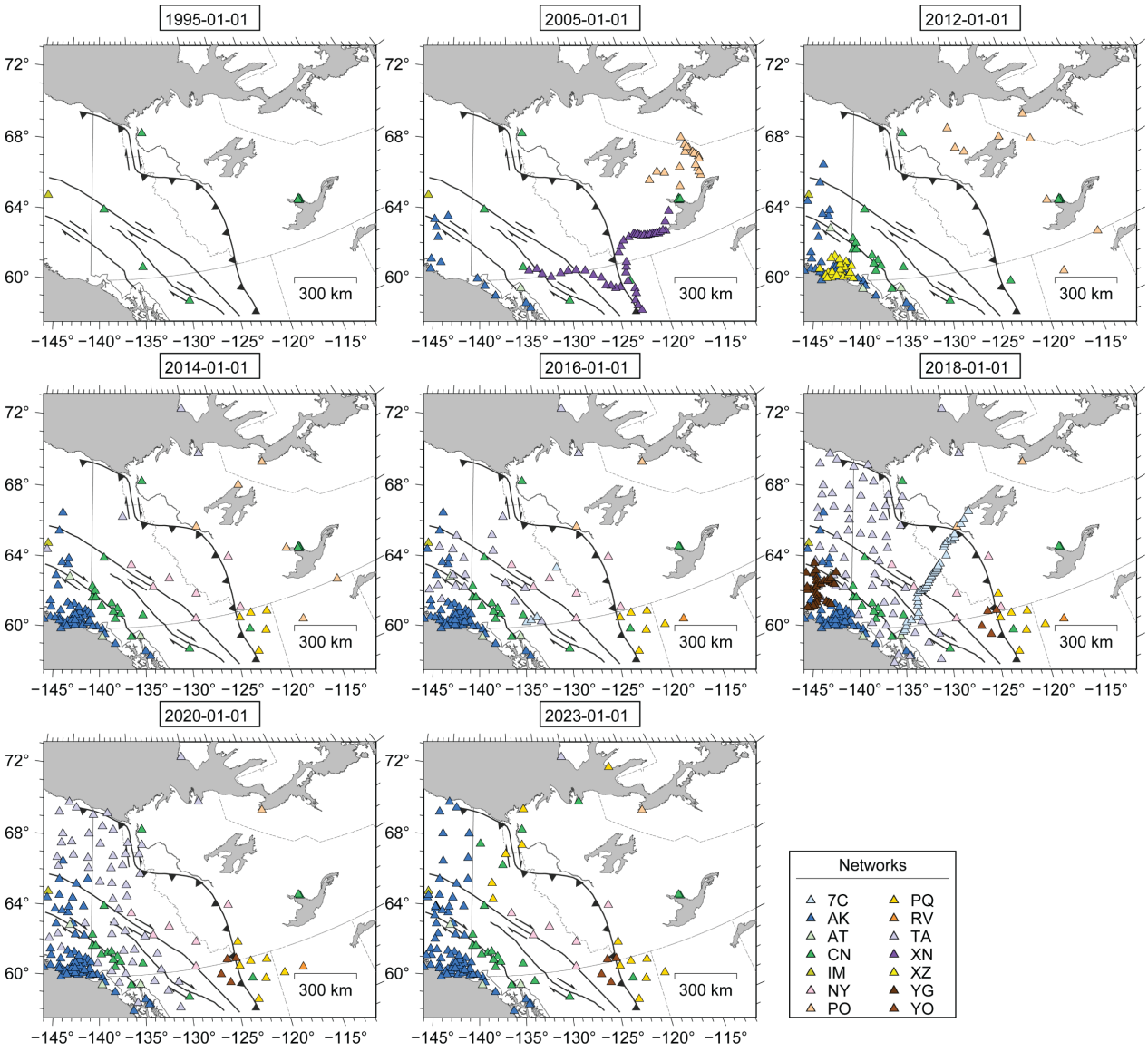

Figure 2. Seismic station coverage across northwestern Canada from January 1995 to January 2023. Triangles depict seismic stations and are color-coded by seismic network.

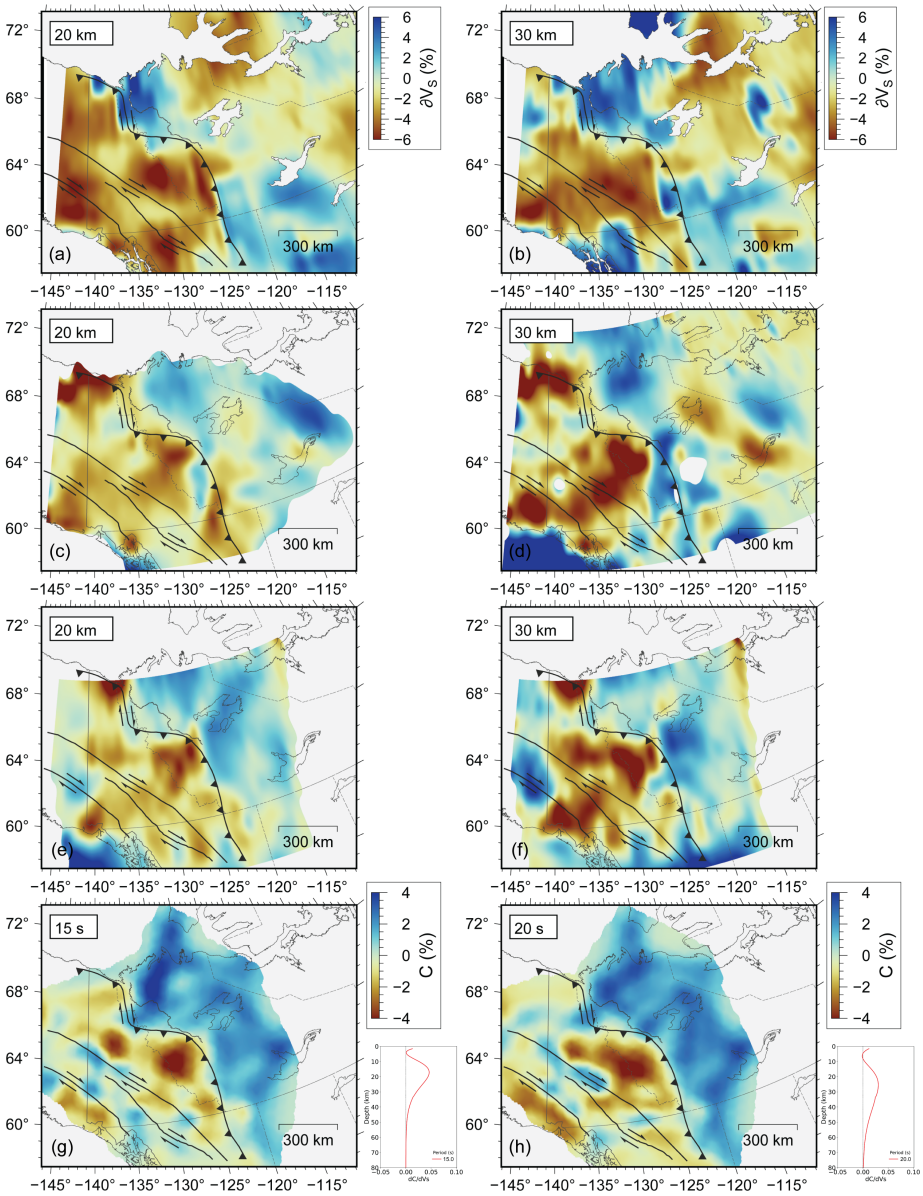

Figure 3. 20 and 30 km depth slices through the *S*-wave velocity models of Kao et al. (2013, a-b), Estève et al. (2021, c-d) and Schutt et al. (2023, e-f). Phase velocity maps at periods of 15 and 20 s from McLellan et al. (2018, g-h) and corresponding phase velocity sensitivity kernels calculated from a simplified version of the global velocity model AK135 (Kennett et al., 1995).

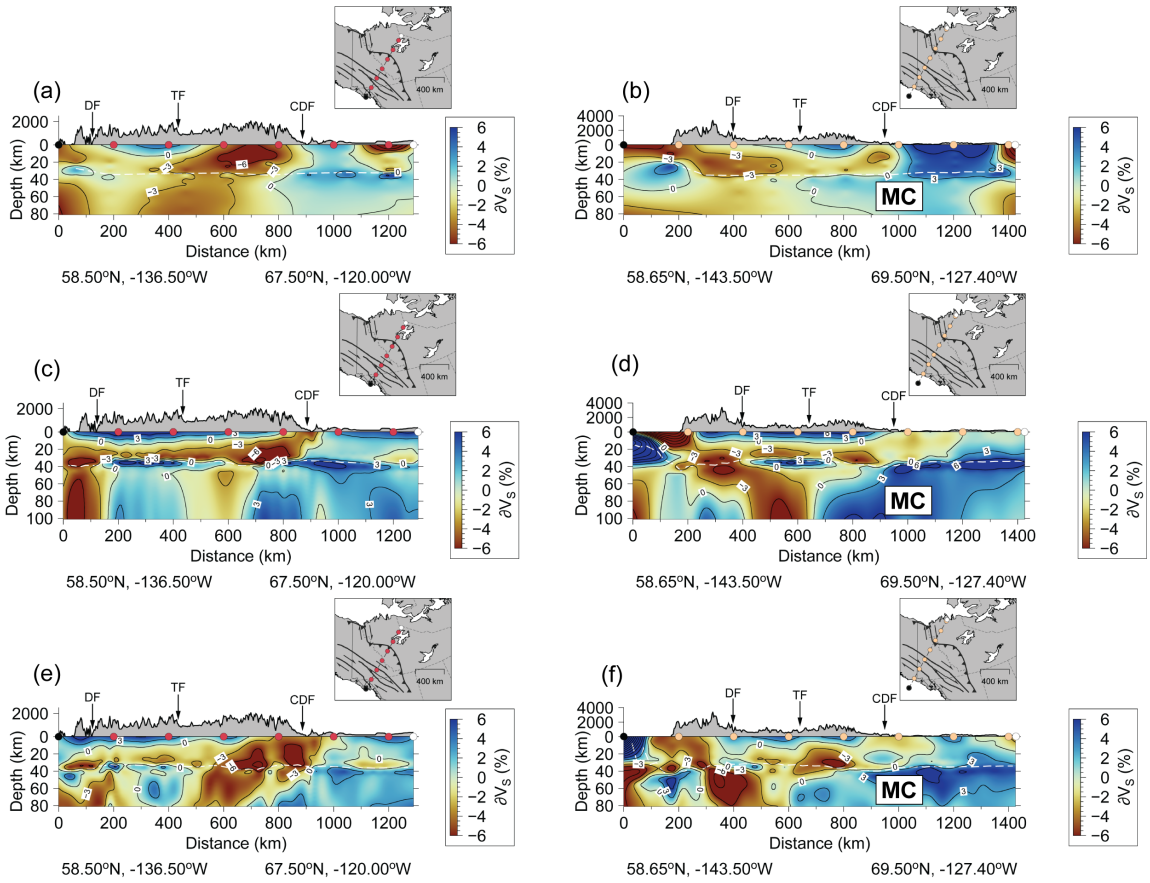

Figure 4. Profiles through the *S*-wave velocity models of Kao et al. (2013, a-b), Estève et al. (2021, c-d) and Schutt et al. (2023, e-f). Inset maps show the profiles locations. Velocity contours are every 3%. White dashed line represents the Moho. Abbreviations: MC, Mackenzie craton.

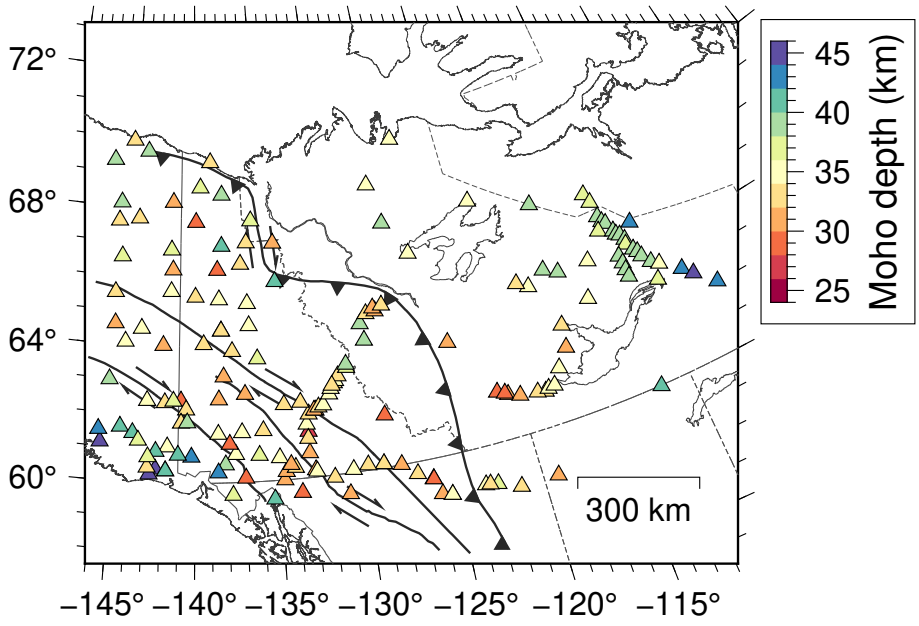

Figure 5. Moho depth estimates across northwestern Canada obtained from Audet et al. (2020); Miller et al. (2018); Postlethwaite et al. (2014).

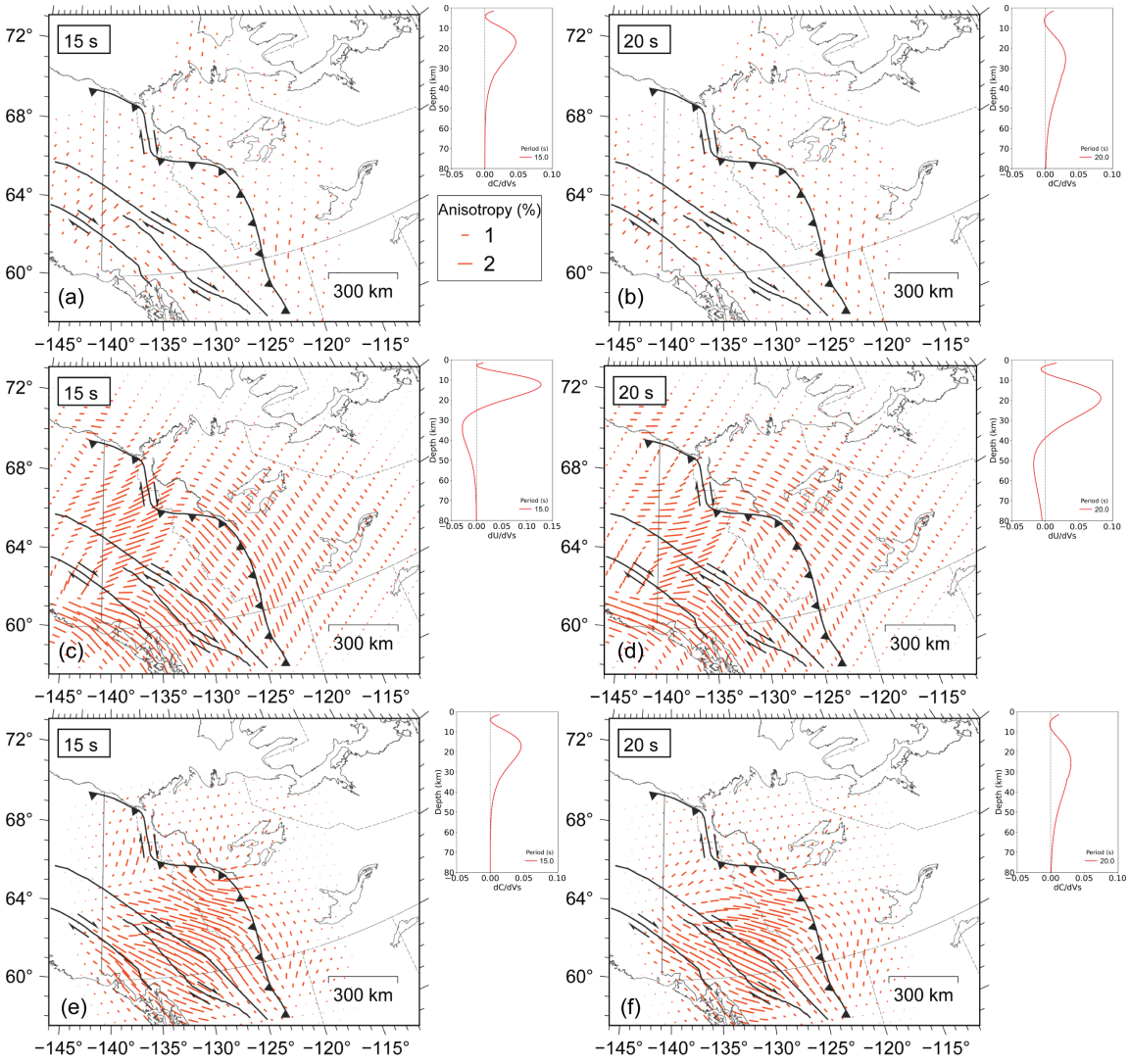

Figure 6. Maps showing azimuthal anisotropy of northwestern Canada at periods of 15 and 20 s from McLellan et al. (2018, a-b), Estève et al. (2021, c-d) and Schutt et al. (2023, e-f). Also shown, phase (a, b, e and f) and group (c, d) velocity sensitivity kernels at 15 and 20 s calculated from a simplified version of the global velocity model AK135 (Kennett et al., 1995).

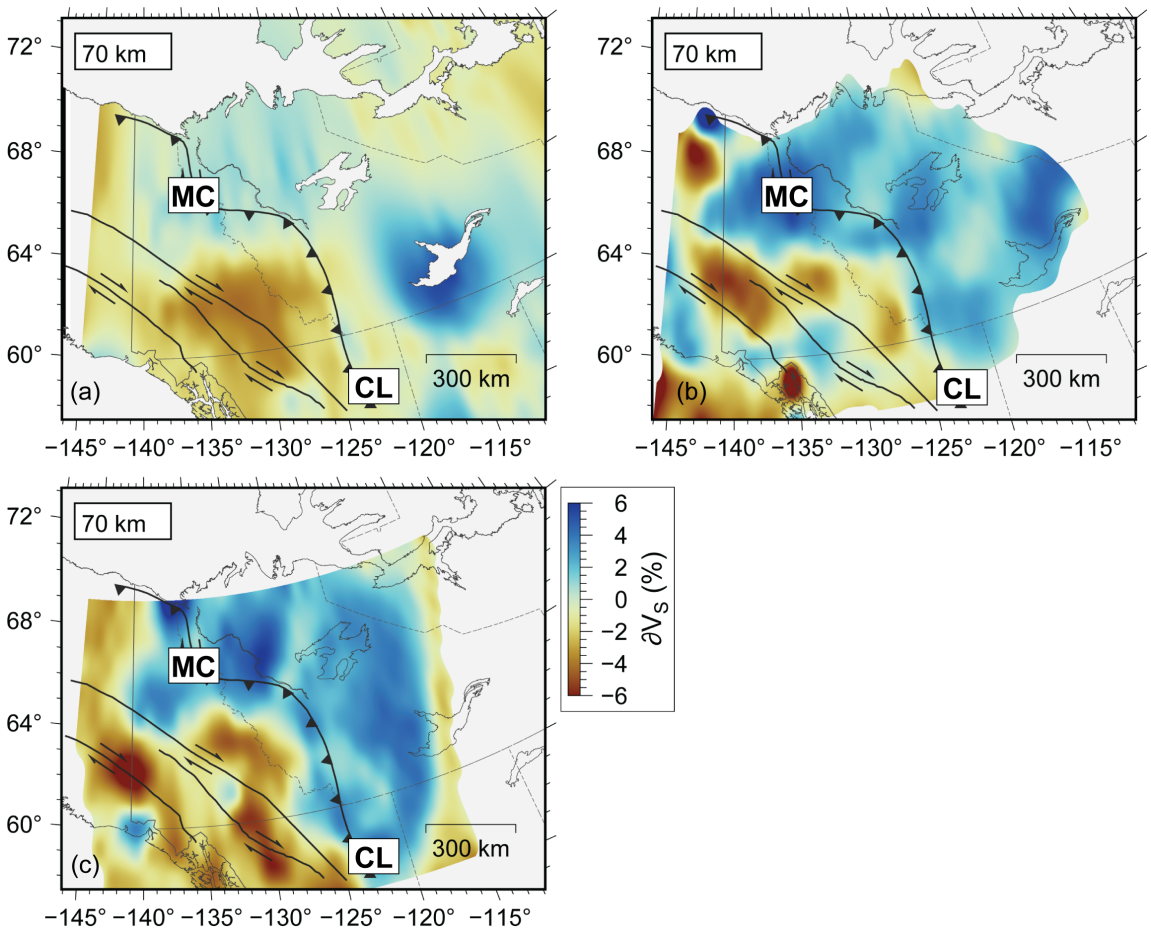

Figure 7. 70-km depth slice through the *S*-wave velocity models of Kao et al. (2013, a), Estève et al. (2021, b) and Schutt et al. (2023, c). Abbreviations: CL, cratonic lithosphere; MC, Mackenzie craton.

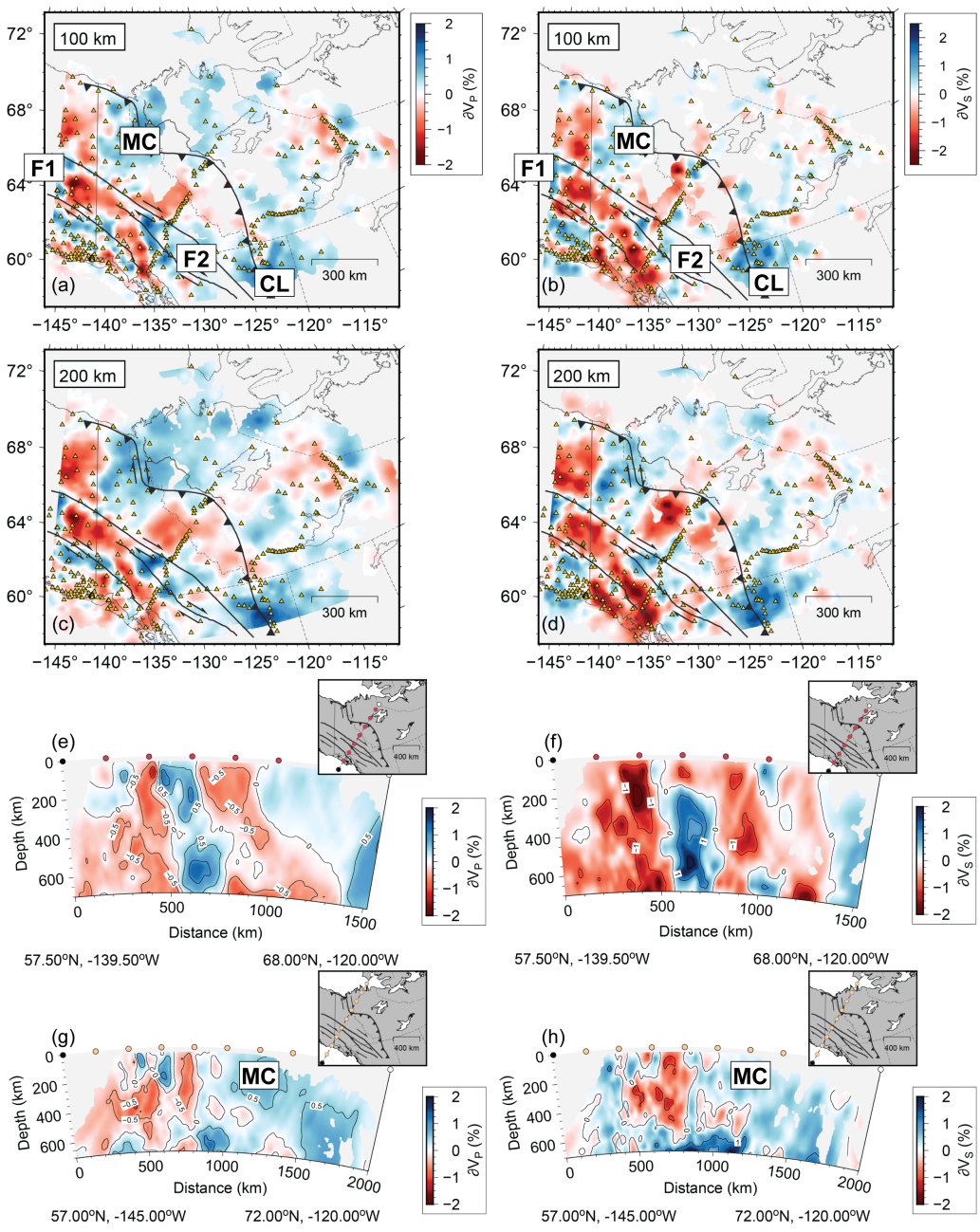

Figure 8. Teleseismic *P*- and *S*-wave tomography models of northwestern Canada (Estève et al., 2020b). 100 and 200-km depth slices through the *P*- (a,c) and *S*-wave (b,d) models. Profiles through the *P*- (e,g) and *S*-wave (f,h) models. Inset maps show the profile locations. Yellow triangles depict seismic stations. Abbreviations: CL, cratonic lithosphere; F1, fragment 1; F2, fragment 2; MC, Mackenzie craton.

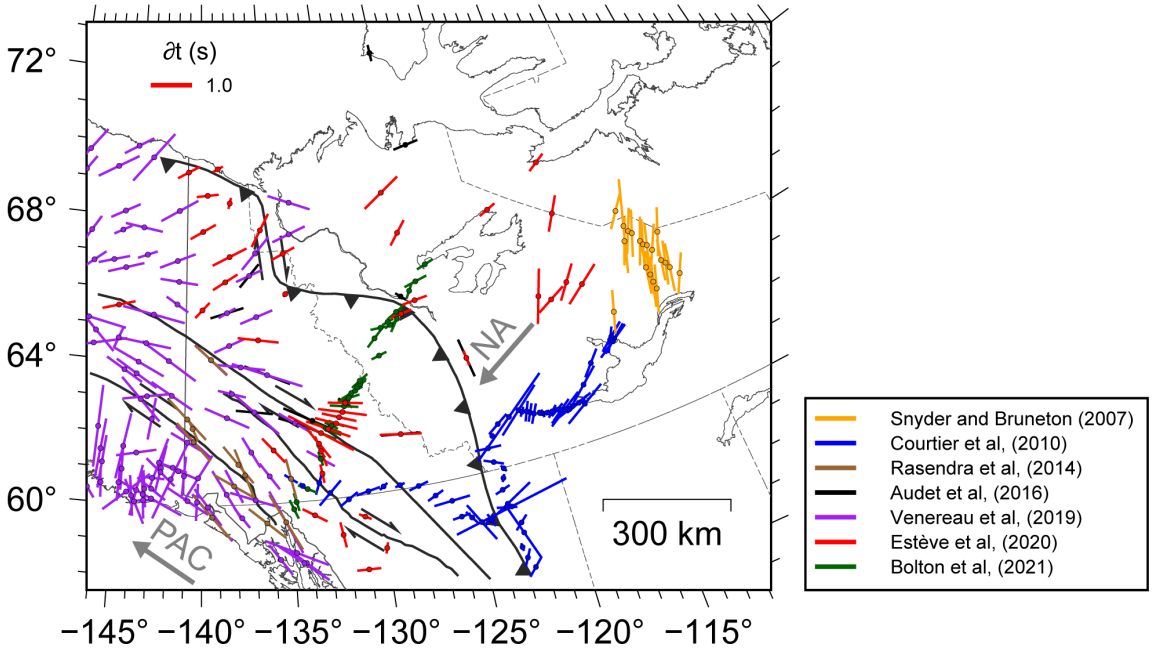

Figure 9. Station average core phase splitting parameters throughout northwestern Canada compiled from Snyder and Bruneton (2007); Courtier et al. (2010); Rasendra et al. (2014); Audet et al. (2016); Venereau et al. (2019); Estève et al. (2020a); Bolton et al. (2021). Colored bars depict the fast-axis direction of propagation scaled by delay time. Grey arrows represent absolute plate motion directions of the North American (NA) and Pacific (PAC) plates from DeMets et al. (2010).

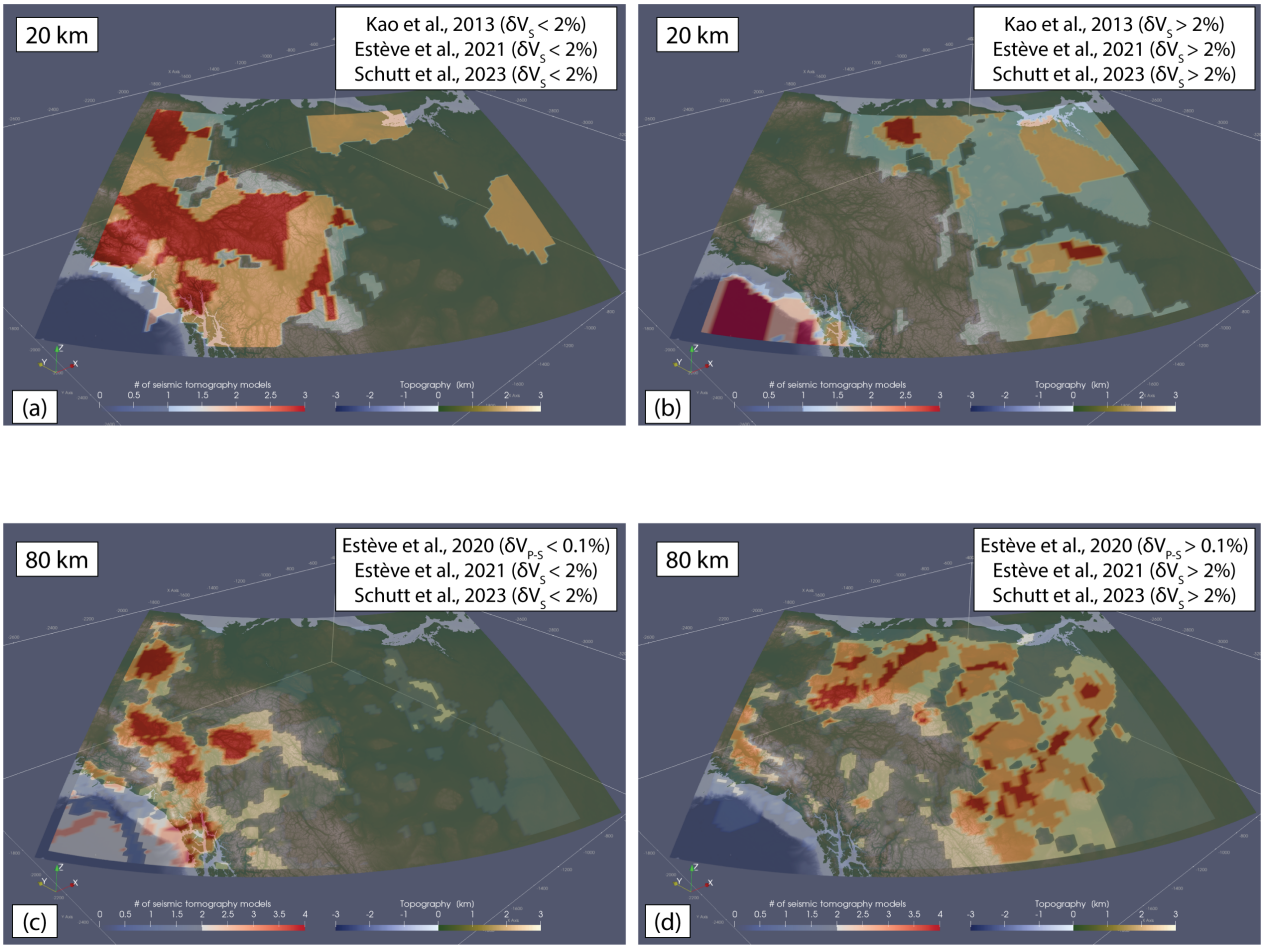

Figure 10. Low-velocity (a,c) and high-velocity (b,d) vote maps at 20 and 80 km depth. Regions where seismic tomography models considered here agree are shown in red. Criteria are shown in top right corner of each panel.